Drug Design, Development and Therapy

Dovepress
Taylor & Francis Group

Open Access Full Text Article

ORIGINAL RESEARCH

The Mechanism of Sijunzi Decoction Suppresses Gastric Cancer Metastasis via the m6A Methyltransferase METTL14 Based on Untargeted Metabolomics Studies and Network Pharmacology Analysis

Xiangnan Li[1,2,*], Linlin Zhao[3,*], Jiluan Wang[3], Tianchi Ma[1,2], Jing Zhou[1,2], Yue Bian[4], Junfu Guo[1,2]

[1]Teaching and Experiment Center, Liaoning University of Traditional Chinese Medicine, Shenyang, Liaoning, People's Republic of China; [2]Shenyang Key Laboratory for TCM Emotional Disorder, Liaoning University of Traditional Chinese Medicine, Shenyang, Liaoning, People's Republic of China; [3]College of Chinese Medicine Integrated with Western Medicine, Liaoning University of Traditional Chinese Medicine, Shenyang, Liaoning, People's Republic of China; [4]Department of Nursing, Shenyang Medical College, Shenyang, Liaoning, People's Republic of China

*These authors contributed equally to this work

Correspondence: Junfu Guo, Liaoning University of Traditional Chinese Medicine, No. 79 Chongshan Road, Huanggu Area, Shenyang, Liaoning Province, People's Republic of China, Tel +86-024-31207185, Email guojunfu@aliyun.com

Background: Sijunzi Decoction (SJZ), a Traditional Chinese Medicine (TCM) formula, is renowned for its capacity to fortify Qi and enhance spleen function. However, additional research is necessary to comprehend the mechanisms beneath the therapeutic potential of SJZ in gastric cancer.

Objective: This research endeavored to analyze how SJZ treats gastric cancer using network pharmacology and experimental validation.

Methods: Liquid chromatography coupled with tandem mass spectrometry (LC-MS/MS) and network pharmacology were applied to systemically clarify the mechanism of SJZ against gastric cancer. We used a xenograft tumor model of gastric cancer and gastric cancer cell lines to explore the effect of SJZ on N6-methyladenosine (m6A) modification. Cell transfection, plate clone formation, scratch migration, and transwell assays were performed in gastric cancer cell lines. The expression levels of m6A enzymes and epithelial-mesenchymal transition (EMT) markers were assessed by Quantitative real-time reverse transcription (RT-qPCR) and Western blotting.

Results: The results revealed 511 active components and 196 targets of SJZ, with 167 targets associated with gastric cancer therapy. Kyoto Encyclopedia of Genes and Genomes (KEGG) enrichment analysis disclosed notable enrichment of pathways related to cancer, metabolism, and immunity. The protein-protein interaction (PPI) network comprised 274 nodes and 2902 edges, whereas the herbal component-target protein-pathway-disease network included 107 nodes and 345 edges, identifying four components with more than 20 putative targets. Experimental assays demonstrated a significant decrease in METTL3 expression following SJZ treatment, whereas the expression level of METTL14 was markedly elevated in the SJZ group across both gastric cancer cell lines and gastric cancer tissues derived from a mouse model ($P<0.01$, $P<0.001$, or $P<0.05$). SJZ inhibited clone formation, migration, and invasion of gastric cancer cells, and EGFR and Vimentin expression via METTL14 ($P<0.05$, $P<0.01$, or $P<0.001$).

Conclusion: METTL14 appears integral to the inhibition of EMT by SJZ as a treatment for gastric cancer.

Keywords: Sijunzi decoction, gastric cancer, METTL14, network pharmacology

Introduction

Gastric cancer constitutes a prevailing malignancy globally and ranks as the third predominant cause of cancer-associated fatalities.[1] Owing to the subtle symptoms of early stage disease and low rates of regular screening, the majority of gastric

Received: 9 December 2024
Accepted: 18 March 2025
Published: 31 March 2025

cancer patients received a diagnosis at advanced tumor stages, resulting in a poor prognosis.[2] Currently, surgery, chemotherapy, radiotherapy, and immunotherapy are recognized as effective treatment modalities for gastric cancer. However, the clinical efficacy of conventional therapies is hindered by tumor invasion and metastasis, resulting in a median overall survival of only approximately eight months for advanced-stage gastric cancer.[3] Consequently, there is growing interest in exploring adjuvant therapies for gastric cancer and investigating their molecular mechanisms for cancer therapy.

In light of TCM theory, gastric cancer is believed to be primarily caused by a deficiency in vital Qi. The main pathogenesis of gastric cancer is attributed to a deficiency of the original Qi and an excess of superficial factors, such as phlegm, blood stasis, heat, and toxins. SJZ, a well-known TCM formula recorded in "Taiping Huimin He Ji Ju Fang" during the Northern Song Dynasty, is noted for its capacity to fortify Qi and enhance the spleen.[4] It is composed of four herbs: *Panax ginseng* (Ren Shen), *Rhizoma Atractylodes macrocephala* (Bai Zhu), *Poria cocos* (Fu Ling), and *Radix Glycyrrhizae* (Gan Cao).[5] Research has indicated that Panax ginseng is capable of prominently enhancing the immune system of the body, leading to an improvement in the overall quality of life.[6] *Rhizoma Atractylodes macrocephala* helps invigorate the spleen to supplement Qi and transmit dampness.[7] *Poria cocos* and *Radix Glycyrrhizae* have been found to have beneficial effects on the spleen and stomach, with polysaccharides and glycyrrhizic acid identified as the main active components, respectively. These compounds exhibit antitumor and immune-enhancing properties.[8,9] Recent clinical investigations has shown that SJZ can effectively prevent and treat malignant tumors, reduce the adverse effects of chemotherapy, enhance immune function, and decrease chemotherapy resistance.[10–13] Furthermore, our antecedent researches have attested to the capacity of SJZ therapy to curb the advancement of gastric cancer in both animal models and cell lines.[14–17] We systematically examined the role of SJZ in gastric cancer using whole transcriptome sequencing and bioinformatic analysis in xenograft tumor mouse model. The results demonstrated that SJZ exerted an anticancer effect in this model by modulating microRNAs and mRNA and their target pathways in tumors.[17,18] Nonetheless, further investigations are requisite to comprehensively apprehend the mechanisms of SJZ in the treatment of gastric cancer.

m6A is a prevalent chemical alteration of eukaryotic mRNAs which plays a role in the development and advancement of tumors.[19] Previous research has indicated that the m6A modification process is controlled by methyltransferases like WTAP/KIAA1429/METTL3/14 (designated as "writers"), eliminated by demethylases FTO and ALKBH5 (termed as "erasers"), and interacts with m6A-binding proteins including YTHDF1/2/3 and IGF2BP1/2/3 (referred to as "readers").-[20] This modification is involved in protein synthesis and signaling pathways that regulate processes related to abnormal proliferation, glycolysis, epithelial–mesenchymal transition (EMT), and drug resistance ultimately contributing to tumor immune evasion and cancer development.[21] METTL3 accelerates gastric cancer angiogenesis by regulating the expressions of hepatoma-derived growth factor (HDGF) or ADAMTS9 through the m6A manner.[22,23] Fan et al found that METTL14 inhibits gastric cancer progression through m6A modification of miR-30c-2-3p/AKT1S1 axis.[19] METTL14-dependent m(6)A modification suppresses CircUGGT2 by interacting with miR-186-3p/MAP3K9 axis to inhibit gastric cancer progression and cisplatin resistance.[24] In addition, Emerging evidence suggests that m6A modification modulates the tumor microenvironment in gastric cancer, affecting immune evasion and therapeutic resistance.[25] Thus, alterations in m6A levels and abnormally expressed m6A regulators probably act as potential clinical therapeutic targets to expand cancer treatment options. However, the effect of SJZ on m6A modifications during progression of gastric cancer remains unclear. In light of this, an untargeted metabolomics study and network pharmacology were employed to investigate the potential targets of SJZ, and in vivo and in vitro experiments were conducted to validate the potential mechanism of action of SJZ against gastric cancer. The work process of this research is depicted in Figure 1.

Materials and Methods

Materials

Panax ginseng (Ren Shen) (certificate specimen number: X071907), *Rhizoma Atractylodes macrocephala* (Bai Zhu) (specimen number: X075027), *Poria cocos* (Fu Ling) (certificate specimen number: X042127), and *Radix Glycyrrhizae* (Gan Cao) (certificate specimen number: X003227) were obtained from the First Affiliated Hospital of Liaoning University of Traditional Chinese Medicine and identified by Dr. Xuetao Li, a pharmaceutical expert in Liaoning University of Traditional Chinese Medicine. TRIzol was purchased from ThermoFisher Scientific (Waltham, MA,

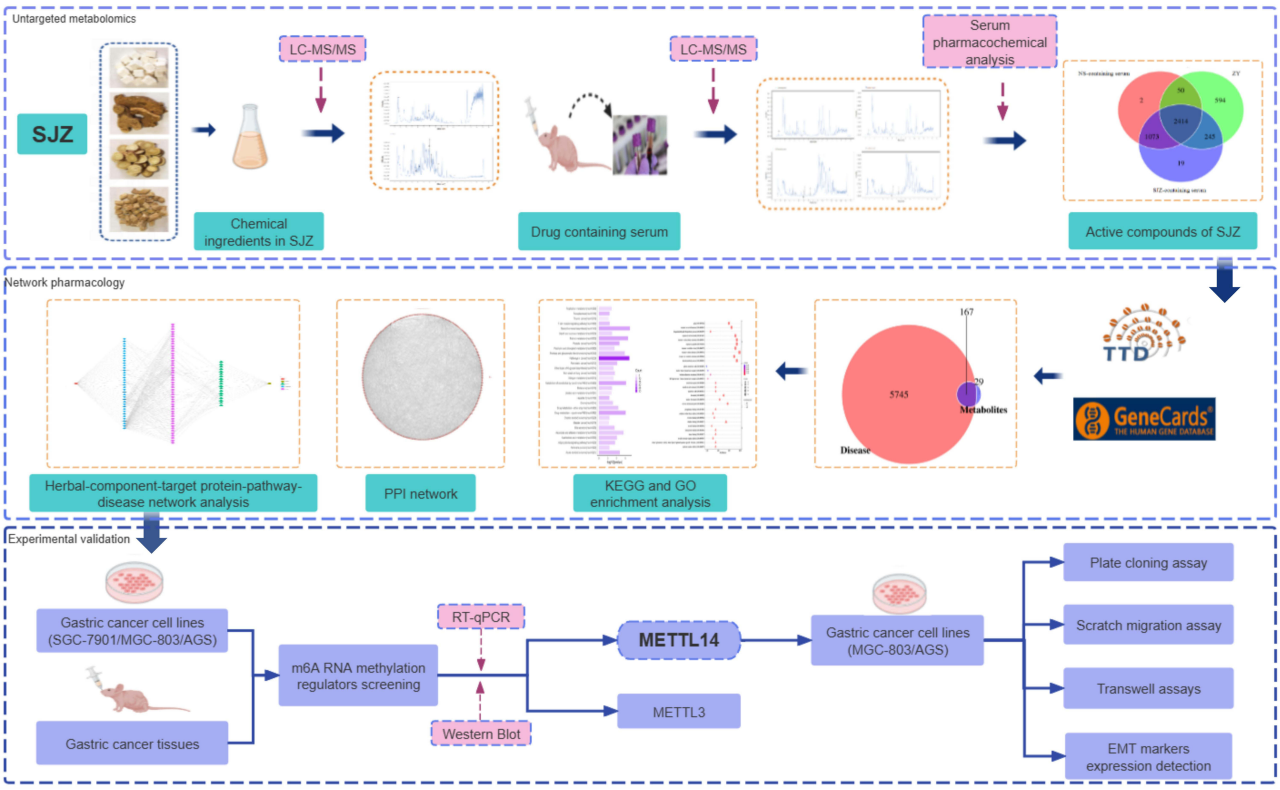

Figure 1 The workflow of this study.

USA). SYBR Green Mixture was supplied from Bimake (Houston, TX, USA). The protein lysis buffer was obtained from Invent Biotechnologies (Plymouth, MN, USA). Bicinchoninic acid (BCA) protein assay kit and secondary antibody (Cat: FDR007) were purchased from Fudebio (Hangzhou, China). METTL3 antibody (Cat: YT8103) and METTL14 antibody (Cat: YT7379) were purchased from Immunoway (USA). The EGFR antibody (Cat: 51071-2-AP) and Vimentin antibody (Cat: 10366-1-AP) were obtained from Proteintech (Wuhan, China). Dulbecco's modified Eagle's medium (DMEM) high sugar medium (Cat: PM150210), AGS special medium (Cat: CM-0022), penicillin-streptomycin (Cat: PB180120), and fetal bovine serum (FBS, Cat: 162410–50) were procured from Wuhan Purcelleno Life Science and Technology Co. Trypsin (0.25%, Cat: SH30042.01) was obtained from Stofan Bioengineering Technology (China). The lentiviruses packaging METTL14 shRNA (targeting sequences: GGGTTACAGAAGATGTGAAGA) were purchased from JiKai Gene (Shanghai, China).

Ethics Statement

All experiments carried out in this research conformed to the ethical norms stipulated in the Declaration of Helsinki, along with national and international directives. Ethical approval to conduct studies using publicly available databases is exempt under the following legislation: item 1 and 2 of Article 32 of "the Measures for Ethical Review of Life Science and Medical Research Involving Human Subjects", which was reviewed by the National Science and Technology Ethics Committee, approved by the State Council of China, and jointly promulgated by the National Health Commission, the Ministry of Education, the Ministry of Science and Technology and the State Administration of Traditional Chinese Medicine on Feb, 18, 2023. The animal experiments received approval from the Animal Core & Welfare Committee of Liaoning University of Traditional Chinese Medicine (Approval numbers: 21010500042019071 and 21000042023082). The animal experiments also strictly adheres to the Guidelines for Ethical Review of Laboratory Animal Welfare (GB/T 35892–2018) (Chinese National Standard) and the Guide for the Care and Use of Laboratory Animals (8th ed., NIH, 2011).

Preparation of SJZ Decoction and Quantity Control

SJZ consists of *Panax ginseng* (Ren Shen, 9g), *Rhizoma Atractylodes macrocephala* (Bai Zhu, 9g), *Poria cocos* (Fu Ling, 9g), and *Radix Glycyrrhizae* (Gan Cao, 6g). The preparation of SJZ followed our prior studies.[17] All the raw herbs underwent decoction thrice and were then concentrated to form a stock solution with a concentration of 2.06 g/mL of the crude drug. Quality control of SJZ liquid was performed using LC-MS/MS.

Nude Mouse Subcutaneous Xenograft Model Construction and Drug Treatment

Nude mouse subcutaneous xenograft model was derived from our previous study.[17] Briefly, BALB/c nude male mice (6–8 weeks old, 20±2 g) from Beijing Huafukang Biotechnology Company [Licence No. SCXK (Beijing) 2019–0008] were subcutaneously injected with 200 μL of SGC-7901 cell suspension (1×10^7 cells/mL). Upon tumors attaining a volume of 100 to 200 cubic millimeters, mice were segregated into two groups: the SJZ group (n=6), receiving 1.32 g/100 g/day of SJZ decoction, and the NS group (n=6), receiving saline. After a three-week treatment duration, blood specimens were obtained through the orbital sinus approach at the first, second, and fourth hours subsequent to gavage. Serum was subsequently isolated through centrifugation for LC-MS/MS analysis. Upon immediate excision of the tumors, they were promptly frozen in liquid nitrogen and then deposited at −80°C for subsequent analysis.

SJZ-Containing Serum

For cell treatment, 20 SPF male rats (8–10 weeks old, 350 ± 50 g) from Liaoning Changsheng Biotechnology Company [Licence No. 211002300043084] were randomly assigned to two groups: NS (n=10) and SJZ (n=10). The NS group received 1 mL/100 g of normal saline daily, while the SJZ group received 1 mL/100 g (0.69 g/100 g body weight) of SJZ daily. On the seventh day, the mice were narcotized by means of 1% pentobarbital sodium, and blood samples were obtained from the abdominal aorta. The collected blood was centrifuged at 2000 g for 15 minutes, 1.5 hours post-drug administration, to separate the serum. The separated serum was then subjected to incubation in a water bath maintained at 56°C for a period of 30 minutes, passed through 0.22 μm filters for the purpose of sterilization, and preserved at −80°C pending further examination.

Cell Culture and Treatment

The human gastric cancer cell lines MGC-803 (BNCC, Shanghai, China), SGC-7901 (BNCC, Shanghai, China), and AGS (Punosai Life Sciences Company, Wuhan, China) were maintained in a 5% CO_2 incubator at 37°C. MGC-803 and SGC-7901 were cultured in DMEM medium with 10% fetal bovine serum (FBS) and 1% penicillin-streptomycin. Following recovery, AGS cells were cultured in AGS-specific medium. The cells were subcultured upon reaching 80% confluence.

MGC-803, AGS, and SGC-7901 cells (1×10^7 cells/well) were assigned to the SJZ group where the cells were exposed to 10% serum containing SJZ or to the NS group where the cells were treated with 10% control rat serum. We treated cells for 48 hours before using them in subsequent experiments.

Metabolites Extraction

SJZ (ZY) decoction in liquid form, as well as serum samples with and without SJZ, were initially thawed on ice. After vortexing for 30 seconds, the samples underwent centrifugation at 13,800 g for 15 minutes at 4°C. Subsequently, 300 μL of the resultant supernatant was aliquoted into a new tube, followed by the addition of 1,000 μL of an extraction solvent containing an internal standard at a concentration of 10 μg/mL. The aliquots were sonicated for five minutes within an ice-water bath. These were then subjected to a temperature of −40°C for one hour before a second centrifugation at 13,800 g for 15 minutes at 4°C. The clarified supernatant was filtered through a 0.22 μm membrane and preserved at −80°C pending UHPLC-MS analysis.

In parallel, plasma samples (400 μL each) were admixed with 40 μL of 2 mol/L hydrochloric acid, vortexed for one minute, and incubated at 4°C for 15 minutes. This procedure was repeated four times. Afterwards, 1.6 mL of acetonitrile was added to each sample, followed by vortexing for five minutes and centrifugation at 13,800 g for five minutes at 4°C. The collected supernatant (1,800 μL) was then transferred into a new tube and evaporated under nitrogen gas. The dry

residues were reconstituted in 150 μL of 80% methanol containing 10 μg/mL of the internal standard, vortexed for five minutes, and centrifuged at 13,800 g for five minutes at 4°C. Finally, 120 μL of the resultant supernatant was transferred to a clean glass vial for subsequent LC-MS analysis.

LC-MS/MS Conditions

LC-MS/MS analysis was conducted in both negative and positive modes within the UHPLC system (Vanquish, Thermo Fisher Scientific), employing a Waters UPLC BEH C18 column (1.7 μm, 2.1×100 mm), with a flow rate of 0.5 mL/min and a sample injection volume of 5 μL. 0.1% formic acid was combined with acetonitrile (A) and water (B) for the preparation of the mobile phase. The multi-step linear elution gradient program was as follows: from 0 to 11 min, 85% to 25% of A; from 11 to 12 min, 25% to 2% of A; from 12 to 14 min, 2% to 2% of A; from 14 to 14.1 min, 2% to 85% of A; and from 14.1 to 16 min, 85% to 85% of A. An Orbitrap Exploris 120 mass spectrometer along with Xcalibur software was utilized to acquire MS and MS/MS data in IDA mode. Each cycle encompassed a mass range of 100 to 1500, screening the top four cycles for the acquisition of MS/MS data. The sheath gas flow rate was 35 Arb; the aux gas flow rate was 15 Arb; the ion transfer tube temperature was 350°C; the vaporizer temperature was 350°C; the full ms resolution was 60000, the MS/MS resolution was 15000, and the collision energy was 16/32/48 in NCE mode; the spray voltage was 4 kV (positive) or 3.8 kV (negative).

Serum Pharmacochemical Analysis of SJZ

We utilized the Human Metabolome Database (http://www.HMDB.ca) for the identification of metabolites. Differential metabolites were discerned through the implementation of both univariate and multivariate analytical methodologies. Metabolites exhibiting a variable importance in the projection (VIP) score of ≥1 in the orthogonal partial least squares discriminant analysis (OPLS-DA), coupled with a *P*-value of less than 0.05 in two-sample *t-tests*, were classified as significantly differential between the two groups. Blood entry prototype components indicate components in ZY and SJZ-containing serum but not in NS-containing serum; Potential blood entry prototype components indicate components in all groups but SJZ-containing serum showed a statistically significant difference from NS-containing serum; metabolites indicate metabolites in SJZ-containing serum but not in NS-containing serum and ZY.

Predicting Targets

The targets of these metabolites were obtained from the ChEMBL (https://www.ebi.ac.uk/chembl/) and TCMIO (http://tcmio.xielab.net) databases, and the metabolites were screened according to their absorption rate (≥ 30%) and drug similarity (≥ 0.18). The disease targets related to gastric cancer were retrieved from GeneCards (https://www.genecards.org/) and TTD databases (http://db.idrblab.net/ttd/).

KEGG and GO Enrichment Analyses

We mapped the genes to the nodes of the Gene Ontology database and used GO (http://www.geneontology.org/) for enrichment analysis. The target proteins that follow biological processes (GO_BP), cellular components (GO_CC), and molecular functions (GO_MF) were presented in three independent ways. KEGG pathway enrichment analysis of overlapping targets was conducted using the KEGG Pathway database (www.kegg.jp/kegg/pathway.html), and $P < 0.05$.

Network Analysis

The PPI of the target protein in the STRING database (https://string-db.org/) for Homo sapiens (human) was determined and a network interaction map of the target protein was constructed. The Cytoscape software (version 3.7.0) was used to construct an herbal-component-target protein-pathway-disease network of SJZ by incorporating herbs, components, target proteins, pathways, and diseases.

RT-qPCR

Briefly, the samples were then exposed to the TRIzol reagent for total RNA extraction. We reverse transcribed 1 μg of RNA to synthesize complementary DNA (cDNA) and subsequently conducted qPCR utilizing SYBR Green Mixture, in accordance with the manufacturer's guidelines. Information of primers are detailed in Table 1. An initial denaturation step was conducted at 95°C for 5 minutes, followed by 40 cycles of 15 seconds at 95°C and 60 seconds at 60°C. GAPDH served as an internal reference. Relative mRNA expression was determined using the $2^{-\Delta\Delta Ct}$ method.

Western Blotting Assay

Cellular lysates were prepared utilizing a protein lysis buffer, and the concentrations of these proteins were quantified through a bicinchoninic acid (BCA) assay. Subsequently, 30 μg of the proteins were resolved via 10% SDS-PAGE and electrophoretically transferred onto PVDF membranes. These membranes were subsequently blocked with a 5% nonfat milk solution for one hour at ambient temperature, followed by an overnight incubation at 4°C with primary antibodies against METTL3, METTL14, EGFR, and Vimentin (1:8000), as well as GAPDH (all diluted 1:1000). Following this, the membranes were exposed to goat anti-rabbit secondary antibodies (diluted 1:10000) in TBST for an additional hour at room temperature. Visualization and analysis of the proteins were facilitated by the Tanon 5200 automated image analysis system (Tanon Science & Technology Co., Ltd, Shanghai, China) and further quantified using ImageJ software (National Institutes of Health).

Table 1 Primer Sequences of for the Genes Investigated in the Present Study

Genes	**Sequence**
KIAA1429	F: 5'- CGATAACTTGATGACCCCAGAA-3'
	R: 5'-ATAACGGCAAGATTCCATTTC-3'
METTL3	F: 5'-CAAGCTGCACTTCAGACGAA −3'
	R: 5'-GCTTGGCGTGTGGTCTTT-3'
METTL14	F: 5'- AAATGCTGGACTTGGGATGATA-3'
	R: 5'- CCCATTTTCGTAAACACACTCTT-3'
WTAP	F: 5'-CTTCCCAAGAAGGTTCGATTGA-3'
	R: 5'-TCAGACTCTCTTAGGCCAGTTAC-3'
ALKBH	F: 5'- CCCGAGGGCTTCGTCAACA −3'
	R:5'- CGACACCCGAATAGGCTTGA −3'
FTO	F: 5'- TGGGTTCATCCTACAACGG −3'
	R: 5'- CCTCTTCAGGGCCTTCAC −3'
GAPDH	F: 5'-ATCATCAGCAATGCCTCC-3'
	R: 5'-CATCACGCCACAGTTTCC-3'
EGFR	F:5'-AACACCCTGGTCTGGAAGTACG-3'
	R:5'-TCGTTGGACAGCCTTCAAGACC-3'
Vimentin	F:5'-GCAAAGATTCCACTTTGCGT-3'
	R: 5'-GAAATTGCAGGAGGAGATGC-3'
Snail	F:5'-TTACCTTCCAGCAGCCCTACG-3'
	R:5'-GCCTTTCCCACTGTCCTCATC-3'
MMP9	F:5'-AGACCTGGGCAGATTCCAAAC-3'
	R:5'-CGGCAAGTCTTCCGAGTAGT-3'
E-cadherin	F:5'-ATTTTTCCCTCGACACCCGAT-3'
	R:5'-TCCCAGGCGTAGACCAAGA-3'
SOX4	F:5'-GGTCTCTAGTTCTTGCACGCTC-3'
	R:5'-CGGAATCGGCACTAAGGAG-3'
S100A4	F:5'-CCCTGGATGTGATGGTGT-3'
	R:5'-GTTGTCCCTGTTGCTGTC-3'
α-SMA	F:5'-CTATGAGGGCTATGCCTTGCC-3'
	R:5'-GCTCAGCCAGTAGTAACGAAGGA-3'

Cell Transfection

During the logarithmic growth phase, MGC-803 and AGS cells were plated evenly in a six-well plate (1×10^5 cells/well). At 37°C, incubate the cells with lentiviral transfection solution and HitransG/P infection solution for 16 to 24 hours, then replace with complete medium. Green fluorescence was observed in 70% of the cells after 48–72 hours to confirm successful transfection, and 4 μg/mL puromycin was used for selection.

Plate Clone Formation Assay

MGC-803 and AGS cells (1×10^3) were cultured in six-well plates, and subjected to incubation for 7–14 days. A medium change was made every 3 days, and the cell status was monitored. The cultivation was ceased when clones became discernible to the unaided eye. Upon removal of the medium, the cells were rinsed with PBS, immobilized with methanol, and tinged with 1% crystal violet. Photographs were captured and the quantity of clones was enumerated by means of ImageJ software.

Scratch Migration Assay

MGC-803 and AGS cells exhibiting robust growth were cultured in six-well plates ($8–9\times10^5$ cells/well) and subjected to drug transfection treatment for 24 hours. Following transfection, a 10 μL pipette tip was used to create scratches on the cell monolayer, which were then washed with PBS and replenished with fresh medium. Images of the scratched areas were captured at 0- and 24-hours post-scratching using a microscope at 100× magnification, with 3–5 fields of view randomly selected for documentation.

Transwell Assays

The cells were subjected to the drug treatment for a period of 24 hours, thereafter being placed in the upper compartment along with matrix gel. Complete medium containing 10% FBS was introduced into the lower compartment, and the cells were subjected to incubation for an additional 24 hours. Subsequent to the incubation, the cells were extracted, rinsed with PBS, fixed using 70% methanol, and stained with 1% crystal violet. The stained cells were examined under an inverted microscope, and 3 to 5 random fields of view at a magnification of 100× were selected for enumeration.

Statistical Analysis

All data were analyzed utilizing GraphPad Prism 8.0. (GraphPad Software, La Jolla, CA, USA) and expressed as mean ± standard error of the mean (SEM). An independent samples t-test was used for comparisons between two groups, whereas one-way analysis of variance (ANOVA) was utilized for comparisons among multiple groups. Statistical significance was defined as $P<0.05$.

Results

Quality Control of SJZ

We conducted LC-MS/MS analysis to determine the preponderant chemical substance in SJZ decoction (ZY) samples. Figure 2A and B showed positive and negative ion chromatograms, respectively. The main chemical components of ZY, including dehydrotumulosic acid, Ginsenoside Rg1, Myristic acid, poricoic acid A, 18 beta-glycyrrhetinic Acid, Glabrolide, naringin, licorice saponin G2, alisol B, chikusetsu saponin Iva, Ginsenoside Ro, (20R)-Ginsenoside Rh1, Ginsenoside Re and Phenylalanine, were shown in Table 2. Three batches of ZY samples were analyzed to ensure the robustness and reliability of the results. The active gradients of the ZY samples were found to be largely consistent across batches. The identification results for the remaining two batches of ZY samples are presented in Figure S1.

Serum Pharmacochemical Analysis

To explore the active ingredients of SJZ absorbed into mouse plasma, We further detected the chemical components of the drug-containing serum by LC-MS/MS. Typical chromatograms were shown in Figure 3. We then compared the total chemical constituents from the ZY and drug-containing serum datasets, and Venn diagram showed that there were 511

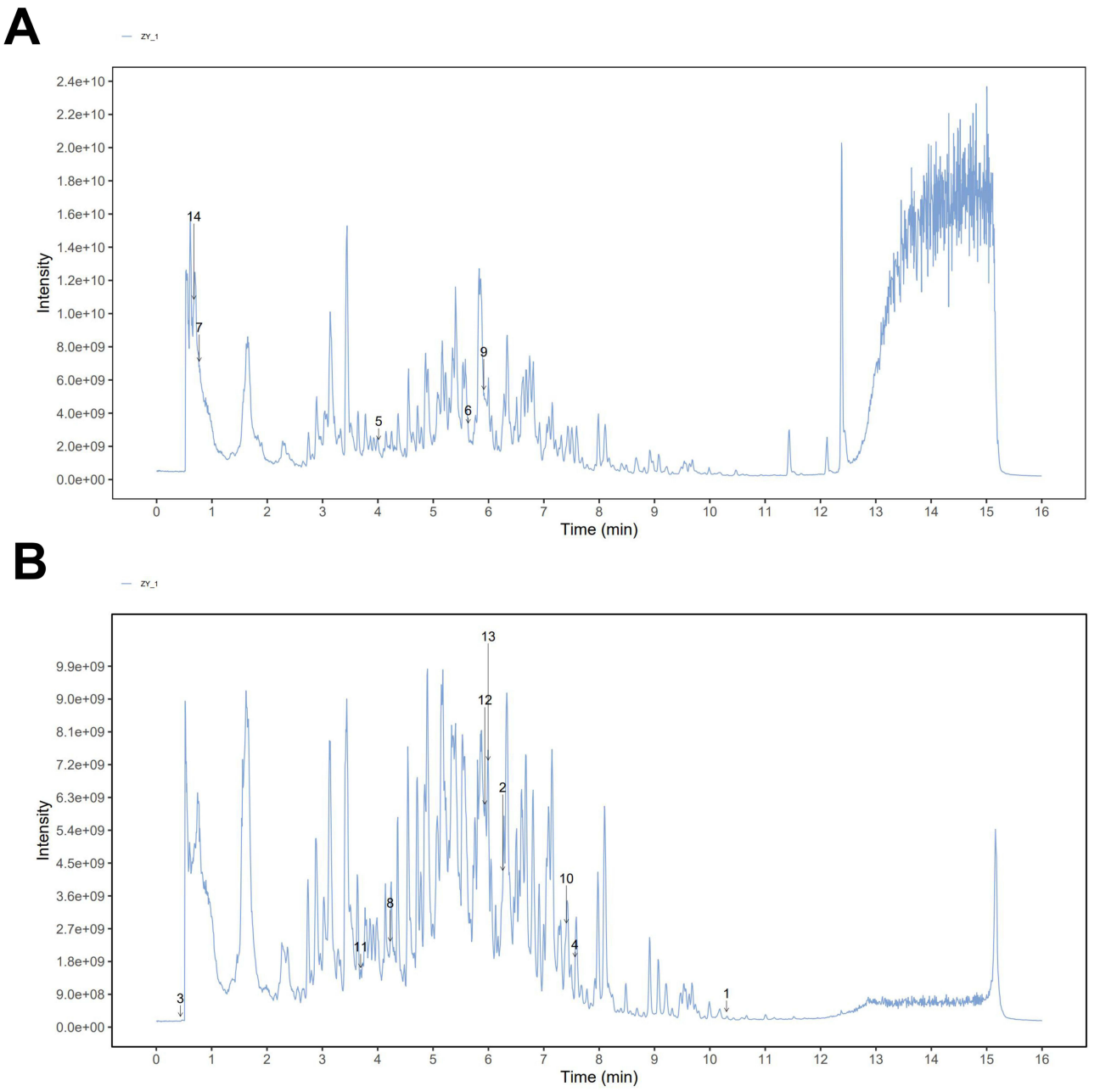

Figure 2 The total ion current chromatograms (TICs) of the SJZ decoction (ZY) samples. ZY samples were detected by LC-MS/MS. ZY samples were shown by TIC in positive (**A**) and negative (**B**) ion modes.

metabolically active compounds, including 245 blood-entry prototype components, 247 potential blood-entry prototype components, and 19 metabolites that could be released into the blood through serum pharmacochemical analysis (Figure 4 and Table S1). Therefore, these blood-entry components may represent potential important substances of SJZ for treatment of gastric cancer.

Prediction and Analysis of SJZ Metabolites and Gastric Cancer-Related Targets

We identified 196 potential targets of metabolically active compounds in SJZ. From GeneCards and TTD databases, we retrieved 5912 gastric cancer-related targets. The results of Venn diagram suggested that 167 overlapping genes were associated with SJZ and gastric cancer targets (Figure 5).

Table 2 The Main Chemical Components Contained in ZY

NO.	Name	herbSet	Formula	mzmed	rtmed	ppm	type	ms2Adduct	MS2
1	Dehydrotumulosic acid	*Poria Cocos*	C31H48O4	483.3482617	618.045	0.541403122	neg	[M-H]-	483.349055;484.345316;53.705743;144.951031;179.395645
2	Ginsenoside Rg1	*Panax ginseng*	C42H72O14	845.49338	375.4805	2.814962495	neg	[M+FA]-	845.405394;846.409455;799.483534;799.510666;93.934598
3	Myristic acid	*Panax ginseng*	C14H28O2	227.2016167	26.1851	1.687204887	neg	[M-H]-	227.200827;227.983802;209.117062;165.129371;71.050367
4	Poricoic acid A	*Poria Cocos*	C31H46O5	497.3263853	453.852	3.246775584	neg	[M-H]-	497.330064;498.330039;55.259219;419.29293;479.319133
5	18 beta-Glycyrrhetinic Acid	*Radix Glycyrrhizae*	C30H46O4	471.3454652	240.8	3.256249644	pos	[M+H]+	471.349125;472.348034;453.33686;52.372792;95.085717
6	Glabrolide	*Radix Glycyrrhizae*	C30H44O4	469.3212114	337.929	20.85696461	pos	[M+H]+	469.329094;470.332597;451.316389;52.148783;95.085606
7	naringin	*Radix Glycyrrhizae*	C27H32O14	619.1422011	46.1449	0.324825225	pos	[M+K]+	619.140191;620.134058;68.795094;70.065013;188.068888
8	Licoricesaponin G2	*Radix Glycyrrhizae*	C42H62O17	837.3936082	253.528	1.92053126	neg	[M-H]-	837.380284;351.055713;113.024406;838.398945;193.03476
9	Alisol B	*Poria Cocos*	C30H48O4	495.346993	354.881	0.014228579	pos	[M+Na]+	495.343994;149.132324;496.351561;435.331186;107.085627
10	Chikusetsu saponin IVa	*Panax ginseng*	C42H66O14	793.4397953	444.475	0.25801903	neg	[M-H]-	793.439799;793.520278;613.380832;569.386821;88.160596
11	Ginsenoside Ro	*Panax ginseng*	C48H76O19	955.494356	221.529	5.90688054	neg	[M-H]-	955.473489;955.508937;956.503308;351.055571;113.024651
12	(20R)-Ginsenoside Rh1	*Panax ginseng*	C36H62O9	683.4389754	356.096	0.035989349	neg	[M+FA]-	637.441974;683.454728;475.373684;101.024348;161.045115
13	Ginsenoside Re	*Panax ginseng*	C48H82O18	945.5437713	359.7305	2.930953881	neg	[M-H]-	945.554503;945.484713;101.024571;946.535301;113.02448
14	PHENYLALANINE	*Rhizoma Atractylodes macrocephala*	C9H11NO2	166.085968	40.4402	0.192792006	pos	[M+H]+	120.080161;166.086895;131.049211;103.054691;121.084621

https://doi.org/10.2147/DDDT.S506702

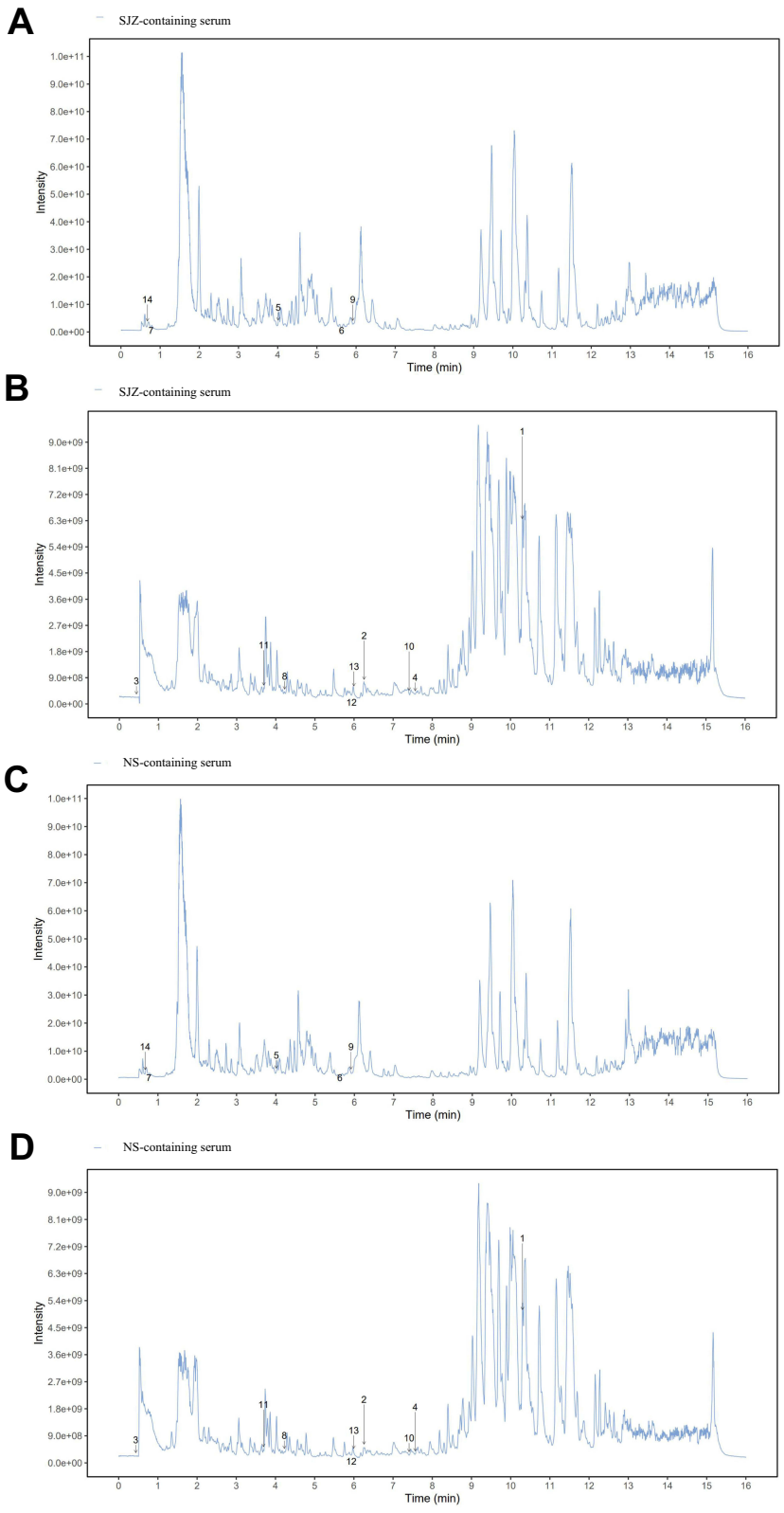

Figure 3 The representative LC-MS/MS TICs of drug-containing serum samples. SJZ-containing serum samples were shown by TIC in positive (**A**) and negative (**B**) ion modes. NS-containing serum samples were shown by TIC in positive (**C**) and negative (**D**) ion modes.

Figure 4 Venn diagram of serum pharmacochemical analysis.

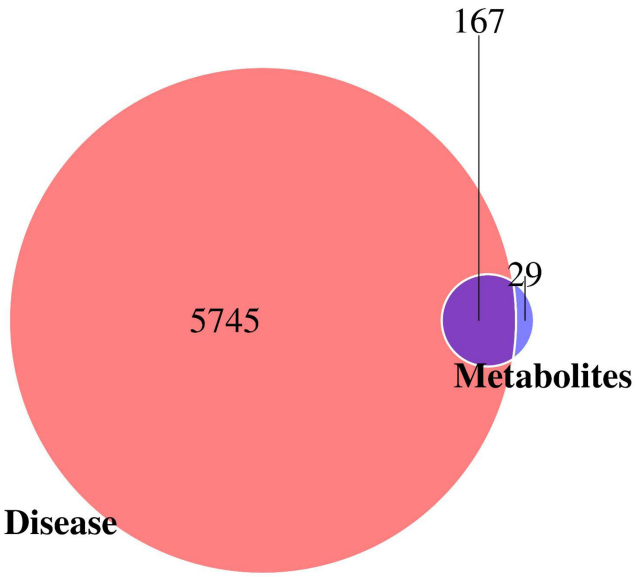

Figure 5 Venn plot of targets analysis.

KEGG Pathway and GO Biological Process Enrichment Analysis

The degree of KEGG enrichment was quantified using enrichment factors (rich factor), *P* values, and the number of genes enriched within each pathway. The targets exhibited significant enrichment in pathways related to cancer, metabolism, and immunity ($P<0.05$), including pathways in cancer (hsa05200), prostate cancer (hsa05215), acute myeloid leukemia (hsa05221), pancreatic cancer (hsa05212), tryptophan metabolism (hsa00380), starch and sucrose metabolism (hsa00500), drug metabolism-other enzymes (hsa00983), ascorbate and aldarate metabolism (hsa00053), T-cell receptor signaling pathway (hsa04660), and others (Figure 6A).

An overview of the GO analyses, highlighting up to ten significantly enriched terms within each of these categories, was presented. The most significantly enriched terms identified were aging (GO:0007568) in BP, plasma membrane rafts (GO:0044853) in CC, and phosphatase binding (GO:0019902) in MF (Figure 6B). These enrichment analyses indicated

https://doi.org/10.2147/DDDT.S506702

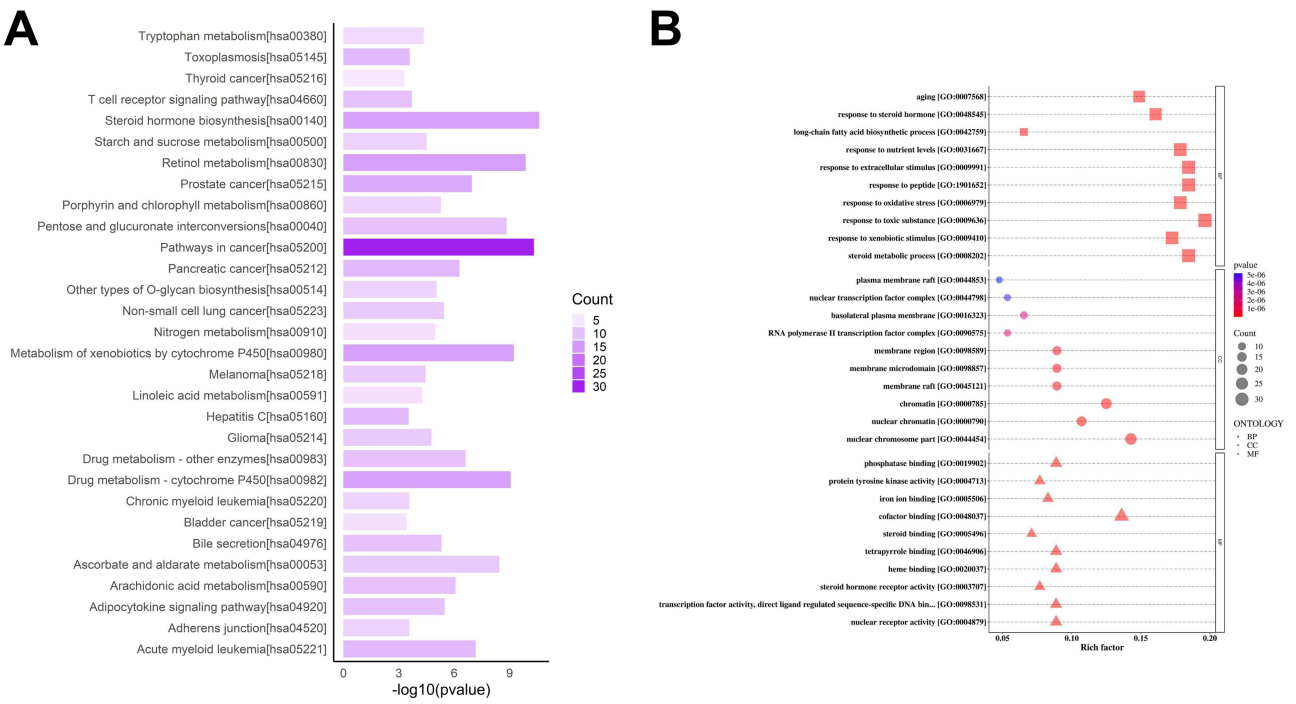

Figure 6 KEGG and GO enrichment analysis. (**A**) KEGG pathway annotation (top 30 enriched pathways), Y-axis label represents signaling pathway and X-axis label represents gene ratio. Gradual changes in color represent probability changes; (**B**) Bubble diagram of GO analysis of target proteins, top 10 enriched terms of biological process (BP), cellular component (CC) and molecular function (MF) were displayed.

that the targets of SJZ were implicated in the regulation of various oncogenic pathways, including those associated with prostate cancer and pancreatic cancer.

PPI Network Analysis

The network consisted of 274 nodes with 2902 edges, whilst the top-10 targets according to node degree were TP53 (119), AKT1 (107), ESR1 (95), EGFR (89), SRC (88), STAT3 (85), HIF1A (82), JUN (80), NFKB1 (76), and PPARG (75) (Figure 7). These protein targets represent the core targets of SJZ against gastric cancer.

Herbal-Component-Target Protein-Pathway-Disease Network Analysis

We analyzed the top 50 blood components that matched their targets and constructed a network with 107 nodes (38 metabolites, 19 KEGG pathways, and 50 potential pharmacodynamic targets) and 345 edges (Figure 8). Topological analysis of the network revealed four components: daidzein (degree=50), kaempferol (degree=30), Biochanin A (degree=28), and isoliquiritigenin (degree=25), which yielded more than 20 putative targets. The network results showed that the mechanism by which SJZ inhibits gastric cancer progression reflects the multi-composition and multi-target characteristics of TCM.

SJZ Modified the Expression of METTL3 and METTL14 in Gastric Cancer Cells

Network pharmacology analysis suggested that SJZ possibly inhibited gastric cancer by targeting the Pathway in cancer via regulating multiple core targets including EGFR, TP53 and STAT3. Recent studies have reported that m6A modifications and m6A regulators play critical roles in tumorigenesis in multiple cancers, and EGFR is one of the m6A targets involved in m6A modifications.[26,27] Thus, m6A regulators KIAA1429, WTAP, METTL3, METTL14, ALKBH, and FTO were detected by RT-qPCR in gastric cancer cell lines MGC-803, SGC-7901, and AGS. As shown in Figure 9A–C, METTL3 mRNA expression was significantly decreased after SJZ treatment, whereas SJZ group exhibited obviously higher levels of METTL14 mRNA expression than NS group ($P<0.05$, $P<0.01$, or $P<0.001$).

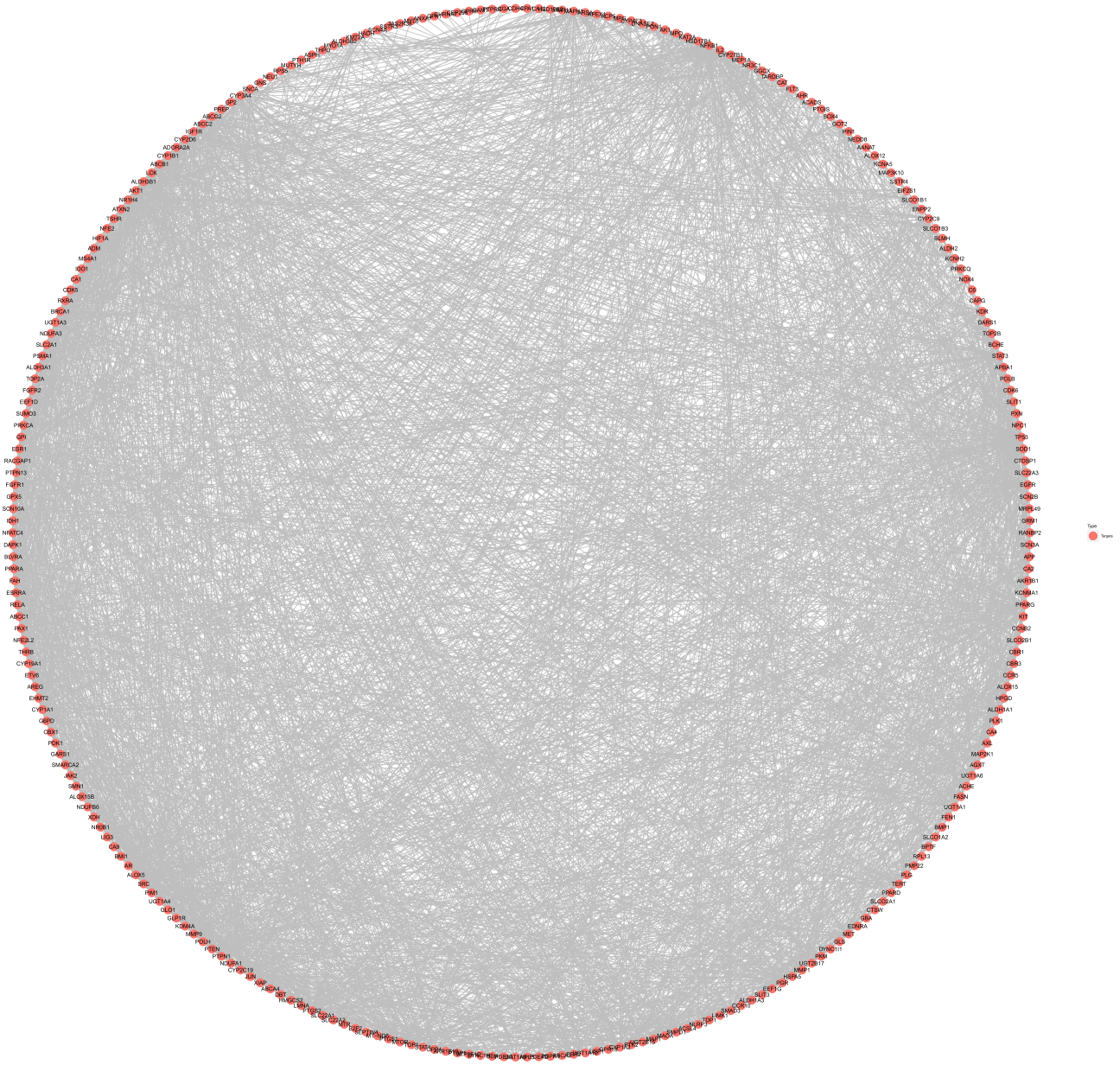

Figure 7 PPI network diagram of cross-target protein.

Moreover, METTL3 and METTL14 protein expression levels were in agreement with their mRNA expression levels ($P<0.05$, $P<0.01$, or $P<0.001$, Figure 9D–I).

SJZ Regulated METTL3 and METTL14 in Gastric Cancer Tissues From Mice Model

Subsequently, the expression of m6A regulators was validated through RT-qPCR and Western blotting in tumor tissues of an SGC-7901 cell xenograft mouse model. In comparison to those in the Model group, the mRNA and protein expression levels of METTL3 were conspicuously downregulated, while those of METTL14 were significantly upregulated in the SJZ group ($P<0.05$, or $P<0.01$, Figure 10). Based on these results, SJZ may be able to target METTL3 or METTL14 for the treatment of human gastric cancer.

https://doi.org/10.2147/DDDT.S506702

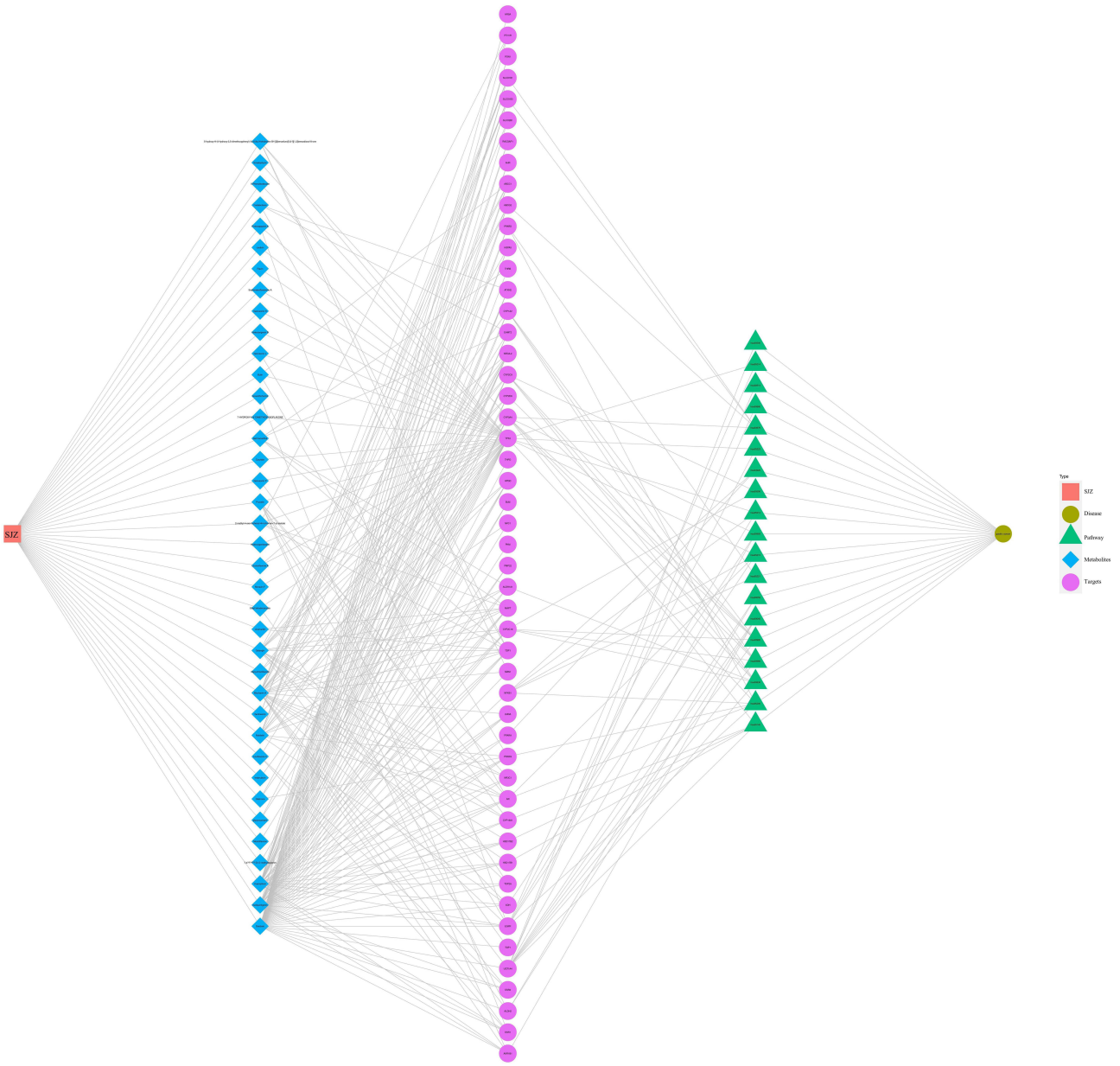

Figure 8 A network pharmacological map of the herbal-component-target protein-pathway-disease.

SJZ Regulated METTL14 to Inhibit Clone Formation of Gastric Cancer Cells

In order to examine the role of METTL14 in gastric cancer treatment by SJZ, shMETTL14 or control was transfected into MGC-803 and AGS cell lines, respectively ($P<0.05$ or $P<0.001$, Figure S2). According to RT-qPCR analysis and Western blotting, the SJZ+shMETTL14 group expressed significantly lower levels of METTL14 than the SJZ+shNC group ($P<0.01$, or $P<0.001$, Figure 11A–C). Colony formation assay was performed to test the effects of SJZ and METTL14 knockdown on gastric cancer cells. It was found that SJZ treatment significantly reduced the clone formation rate of MGC-803 and AGS cells, while SJZ+shMETTL14 group exhibited a notable increase compared to control ($P<0.05$, or $P<0.001$, Figure 11D–G). This indicated that SJZ suppressed the clone formation ability of gastric cancer cells through METTL14.

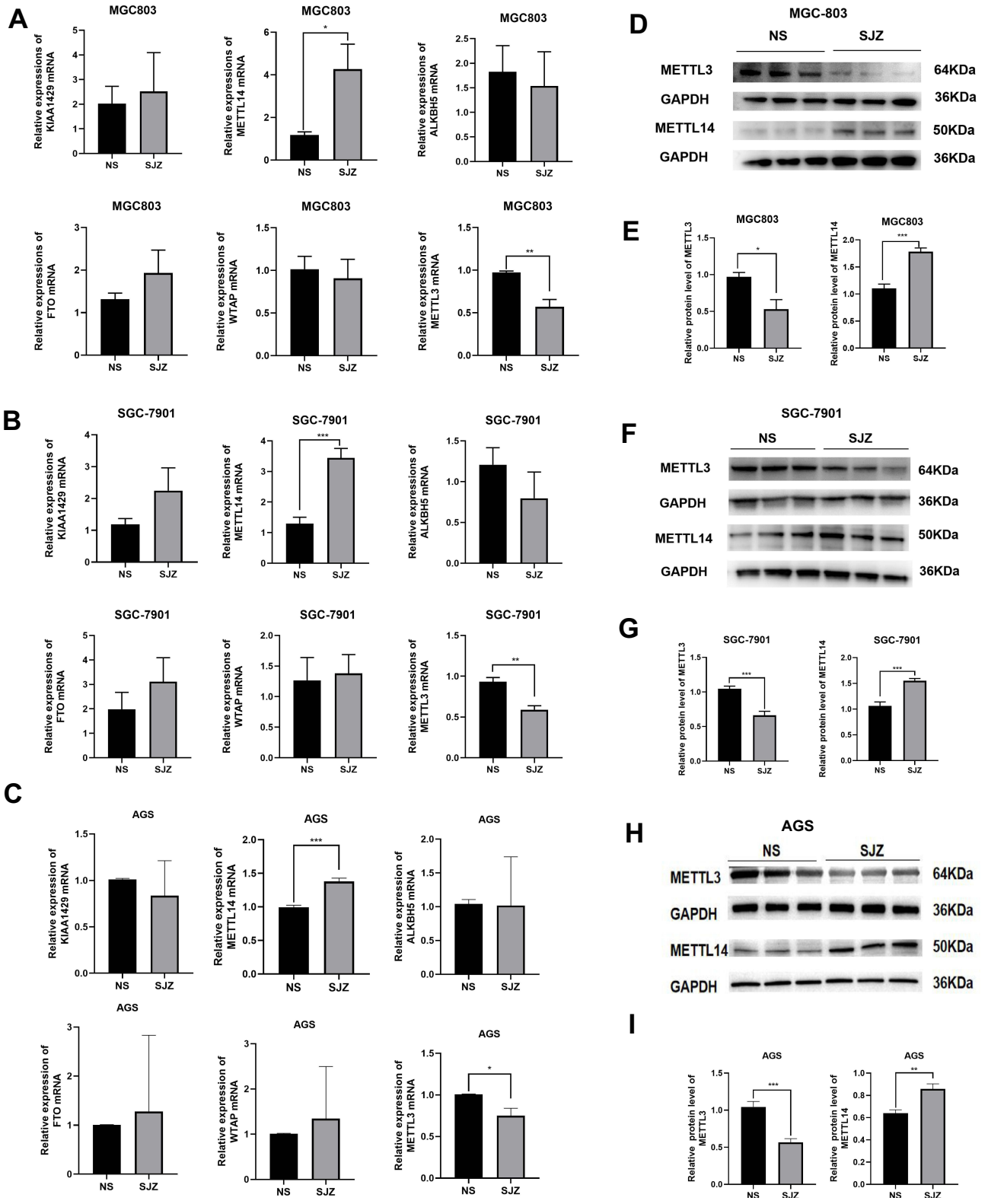

Figure 9 Effect of SJZ-containing serum on modulation of m6A RNA methylation regulators in gastric cancer cell lines. The mRNA expressions of KIAA1429, WTAP, METTL3, METTL14, FTO and ALKBH detected by RT-qPCR in MGC-803 cells (**A**), SGC-7901 cells (**B**) and AGS cells (**C**). The protein expressions of METTL3 and METTL14 in MGC-803 cells (**D** and **E**), SGC-7901 cells (**F** and **G**) and AGS cells (**H** and **I**) determined by Western blotting. The data are stated as the means±SEM, n=5. **P*<0.05, ***P*<0.01, ****P*<0.001 compared to control. Cells were treated by NS-containing serum (NS) and SJZ-containing serum (SJZ).

https://doi.org/10.2147/DDDT.S506702

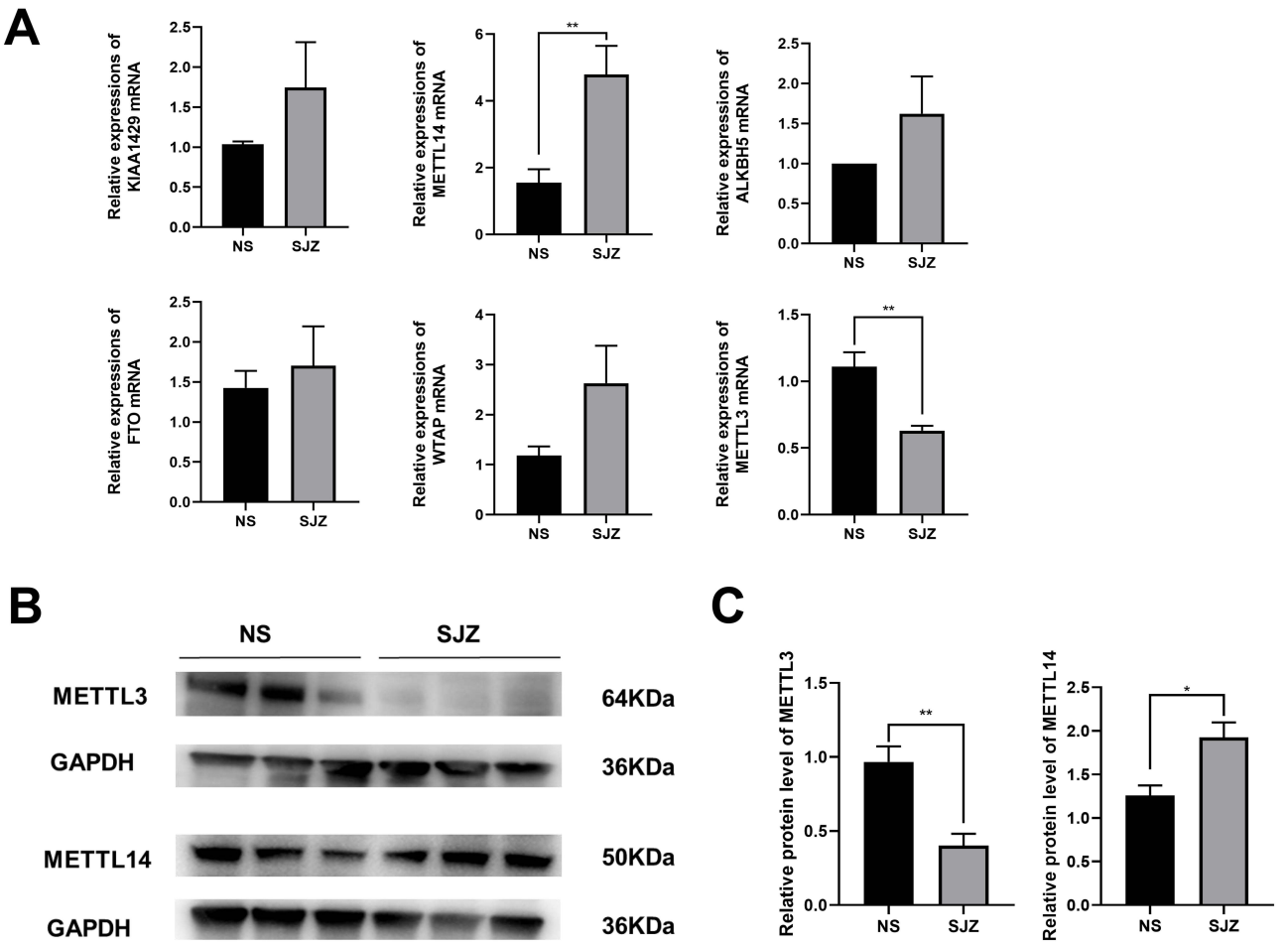

Figure 10 Effect of SJZ on modulation of m6A RNA methylation regulators in gastric cancer tissues. (**A**) The mRNA expressions of KIAA1429, WTAP, METTL3, METTL14, FTO and ALKBH detected by RT-qPCR. (**B** and **C**) The protein expressions of METTL3 and METTL14 were determined by Western blotting. The data are stated as the means±SEM, n=5. **P*<0.05, ***P*<0.01 compared to control. Tissues were obtained from NS group (NS) and SJZ group (SJZ).

SJZ Regulated METTL14 to Inhibit Gastric Cancer Cells Migration

As illustrated in Figure 12, knockdown of METTL14 reversed the inhibitory effects of SJZ on MGC-803 and AGS cells ($P<0.05$, $P<0.01$ or $P<0.001$). The finding indicated that reduced expression of METTL14 might partially mitigate the inhibitory effects of SJZ on cell migration in gastric cancer cells.

SJZ Regulated METTL14 to Inhibit Gastric Cancer Cells Invasion

The invasive potential of gastric cancer cells was evaluated utilizing a transwell assay. These findings indicated that treatment with SJZ significantly inhibited the invasion of MGC-803 and AGS cells, while the knockdown of METTL14 was associated with an increased invasive capacity of gastric cancer cells ($P<0.05$, or $P<0.001$, Figure 13). According to these findings, SJZ might exert its inhibitory effects on the invasive ability of gastric cancer cells through modulation of METTL14.

SJZ Repressed Expression of EGFR and Vimentin in Gastric Cancer Cells via METTL14

To detect the effect of SJZ on EMT in gastric cancer cell lines, the mRNA expression of the EMT markers E-cadherin, S100A4, MMP-9, α-SMA, Snail, SOX4, EGFR and Vimentin was detected using RT-qPCR. After SJZ treatment, both cell lines expressed lower levels of EGFR and vimentin, but the effect was partially reversed by knockdown of METTL14 ($P<0.05$, $P<0.01$, or $P<0.001$, Figure 14A and B). In alignment with our RT-qPCR results, the SJZ group exhibited remarkably lower protein levels of EGFR and Vimentin than the NS group. Conversely, in the SJZ+shMETTL14 group, the levels of

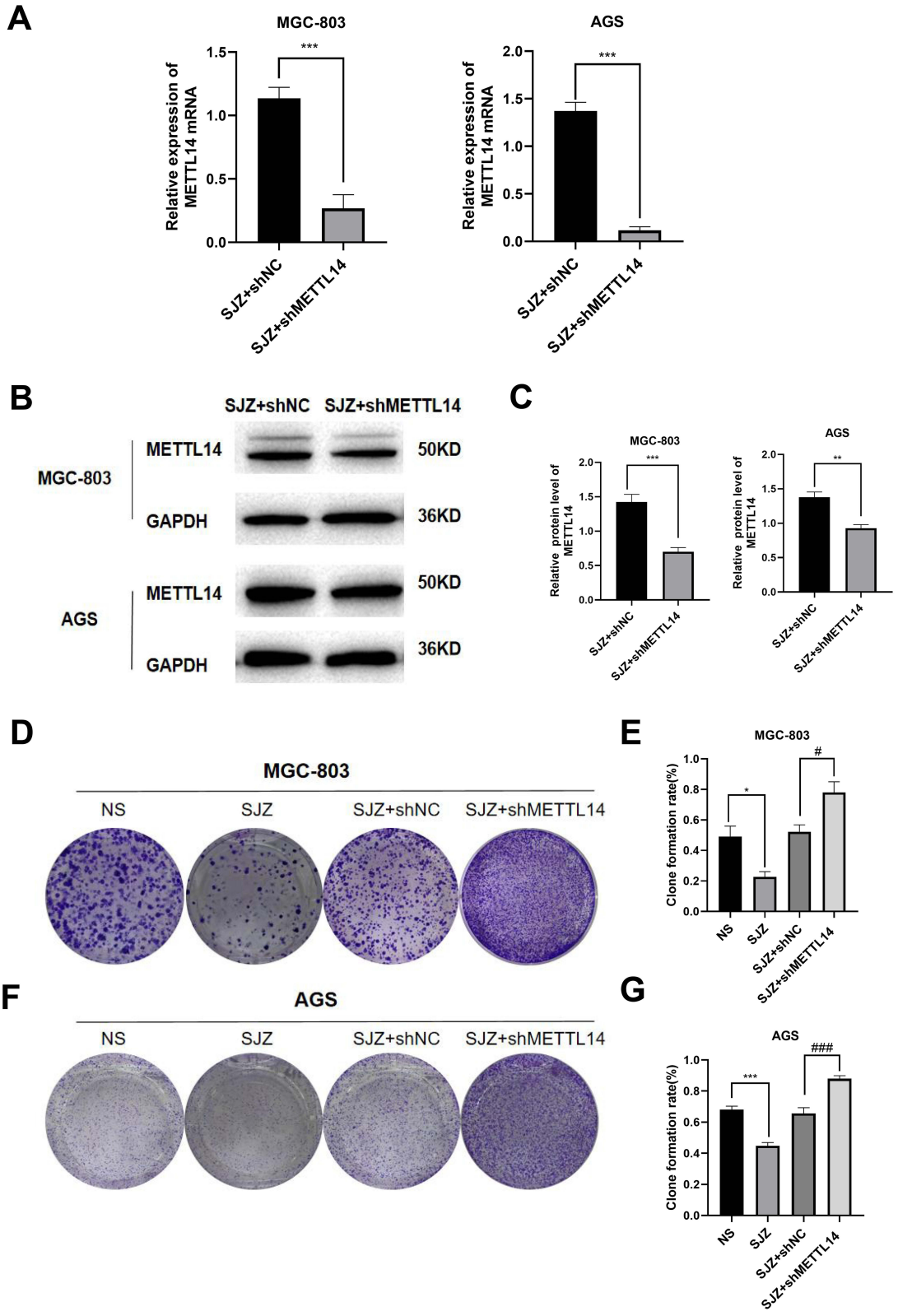

Figure 11 SJZ inhibits clone formation of gastric cancer cells via METTL14. (**A**) The mRNA expression of METTL14 in MGC-803 and AGS cells were detected by RT-qPCR. (**B** and **C**) The protein expressions of METTL14 in MGC-803 and AGS cells were determined by Western blotting. Representative images of plate clone formation assay of MGC-803 (**D**) and AGS (**F**) cells treated with SJZ, NS, or SJZ after transfection of shMETTL14 or shNC. Clone formation rate of MGC-803 (**E**) and AGS (**G**)cells after treatment. The data are stated as the means±SEM, n=5. **P*<0.05, ***P*<0.01, ****P*<0.001, $^{\#}P$ <0.05, $^{\#\#\#}P$ <0.001 compared to control.

https://doi.org/10.2147/DDDT.S506702

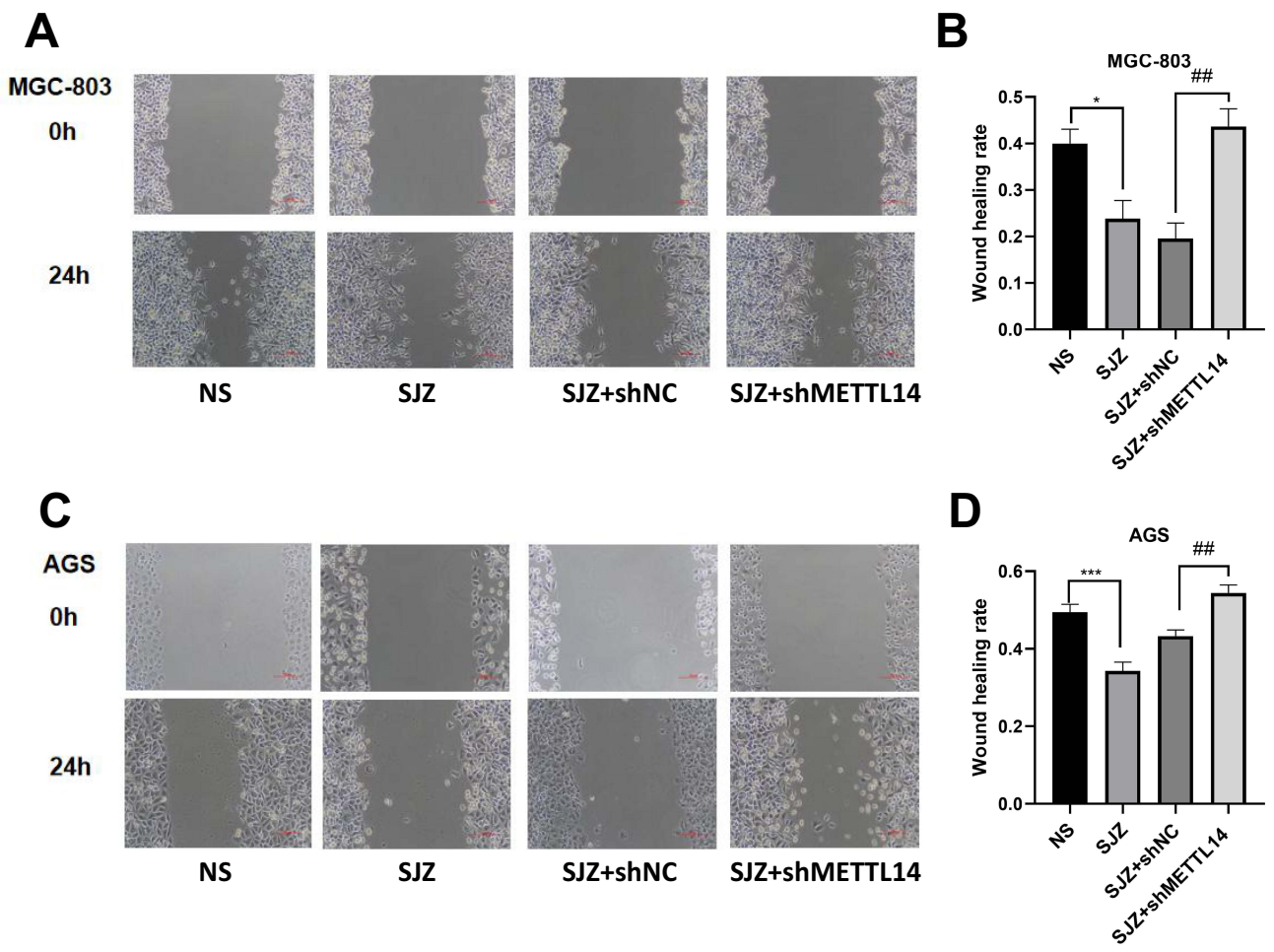

Figure 12 SJZ inhibits gastric cancer cells migration via METTL14. Representative images of cell scratch assay of MGC-803 (**A**) and AGS (**C**) cells treated with SJZ, NS, or SJZ after transfection of shMETTL14 or shNC at 0-h and 24-h; magnification, ×100. Relative covered area of MGC-803 (**B**) and AGS (**D**)cells after treatment. The data are stated as the means±SEM, n=5. **P*<0.05, ****P*<0.001, ##*P*<0.01 compared to control.

EGFR and Vimentin proteins were markedly elevated relative to the control (*P*<0.05, *P*<0.01, or *P*<0.001, Figure 14C–F). These findings suggested that SJZ inhibited EMT markers in gastric cancer cells by modulating METTL14 expression.

Discussion

There has been evidence that SJZ can treat gastrointestinal diseases, including gastric cancer.[5,28–34] Our previous studies utilizing gastric adenocarcinoma SGC7901 murine models have demonstrated the significant antitumor effects of SJZ.[17] However, the intricate chemical composition and complex interactions among multiple components pose challenges to the investigation of the molecular mechanism of SJZ. Therefore, our goal was to determine the underlying mechanisms of SJZ and identify novel therapeutic targets against gastric cancer using LC-MS/MS, serum pharmacochemical analysis, network pharmacology, and in vitro and in vivo experiments.

Previous studies have demonstrated the detection of blood-entering components of SJZ in rat serum samples using HPLC-Q-TOF-MS for the treatment of Alzheimer's disease.[35] In the present study, serum pharmacochemical analysis identified 511 potentially active ingredients of SJZ, including 19 metabolites absorbed into the bloodstream. Furthermore, while there have been investigations into the efficacious chemical constituents of SJZ, limited research has been conducted on gastric cancer biomarkers in nude mouse models, particularly utilizing untargeted metabolomic methodologies.[5,36] Our analysis revealed 196 targets of active metabolites of SJZ and 167 shared genes associated with both SJZ and gastric cancer targets.

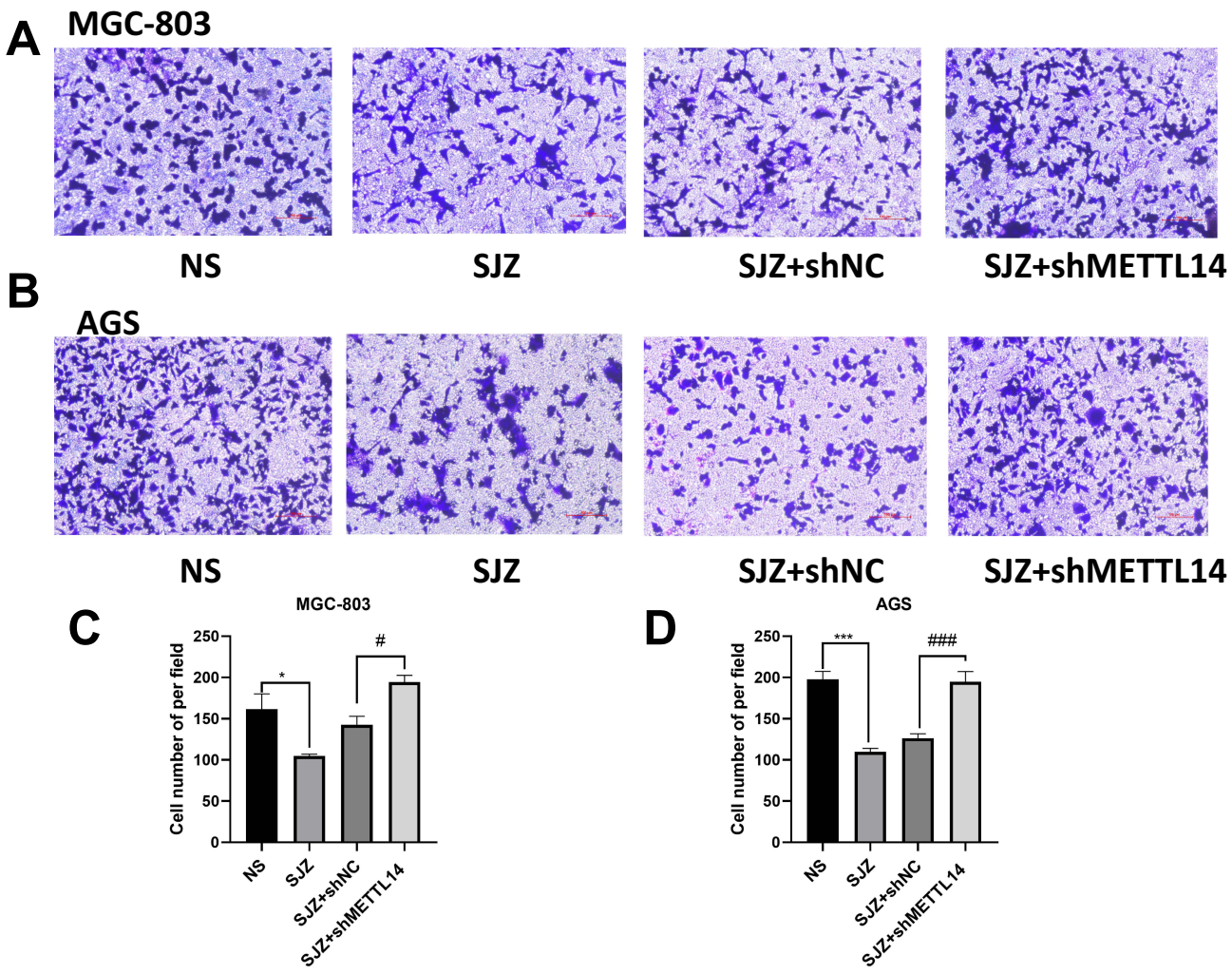

Figure 13 SJZ inhibits gastric cancer cells invasion via METTL14. Representative images of cell scratch assay of MGC-803 (**A**) and AGS (**B**) cells treated with SJZ, NS, or SJZ after transfection of shMETTL14 or shNC at 48-h; magnification, ×100. (**C** and **D**) The mean number of invaded cells from three randomly selected fields under the microscope. The data are stated as the means±SEM, n=5. **P*<0.05, ****P*<0.001, #*P*<0.05, ###*P*<0.001 compared to control.

TCM, characterized by its complex system of multiple components, targets, and pathways of action, aligns with a holistic approach for treating diseases.[37] Network pharmacology serves as a conduit for investigating the interplay between TCM and contemporary pharmacology.[38–40] Through the construction of compound-target and target-disease networks, we identified several critical nodes that may serve as pivotal points for the therapeutic efficacy of SJZ. The results of KEGG and GO enrichment analyses revealed that SJZ targets were significantly enriched in pathways related to cancer, metabolism, and immunity. This suggests that SJZ may exert antitumor effects by modulating cancer-related pathways, including those involved in tumor metastasis and stemness.

m6A, the most prevalent epigenetic modification of RNA, plays a critical role in driving abnormal transcription and translation processes that contribute to cancer initiation and advancement.[25] Recently, a number of studies have centered on the regulatory impacts of TCM via m6A modification, and it has been shown that TCMs can regulate methyltransferases and demethylases in some diseases.[41–43] As of yet, the epigenetic effects of SJZ on m6A modification remains poorly understood. In present research, we investigated the m6A regulators KIAA1429, WTAP, METTL3, METTL14, ALKBH, and FTO by RT-qPCR in xenograft mouse models and three gastric cancer cell lines. Western blotting was performed to validate RT-qPCR results. Our findings indicated that the expression levels of METTL3 and METTL14 were altered by SJZ, suggesting the potential involvement of m6A in the anticancer mechanism of SJZ. Specifically,

https://doi.org/10.2147/DDDT.S506702

METTL3, a key RNA methyltransferase highly expressed in gastric cancer tissues and cells,[44] significantly decreased following SJZ treatment, indicating its potential as a therapeutic target of SJZ.

METTL14 inhibits the progression of gastric cancer, and has been proven to be a biomarker for its diagnosis and prognosis.[19,45] Our study revealed an upregulation of METTL14 in gastric cancer tissues and cells following treatment with SJZ, indicating that SJZ may exert its anticancer effects through the regulation of METTL14. Furthermore, we found that SJZ suppressed clone formation, migration, and invasion of gastric cancer cells and EGFR and Vimentin expression by modulating METTL14. Therefore, we hypothesized that SJZ inhibits gastric cancer cell progression by upregulating METTL14. Additionally, our previous study reported that the antitumor effects of SJZ on gastric cancer may be partly attributed to the modulation of miRNA expression and their associated pathways.[17] The writer and eraser enzymes play a role in pri-miRNA methylation, leading to accelerated maturation by recruiting DGCR8 and m6A reader HNRNPA2B143.[46] It has also been demonstrated that miRNAs alter m6A regulator translation to influence m6A modification function in return.[47] This suggests that m6A may serve as a novel mechanism by which SJZ regulates

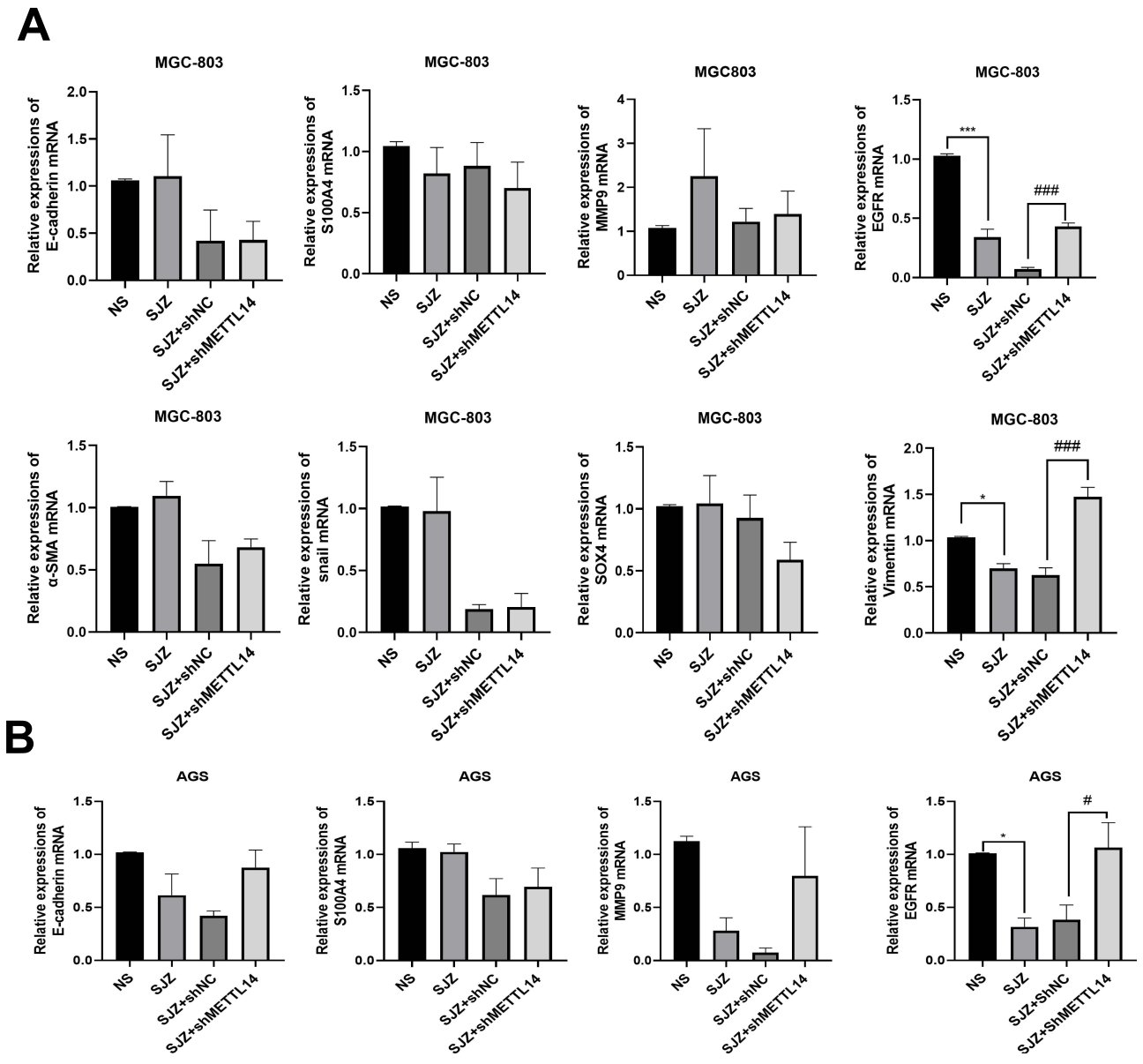

Figure 14 Continued.

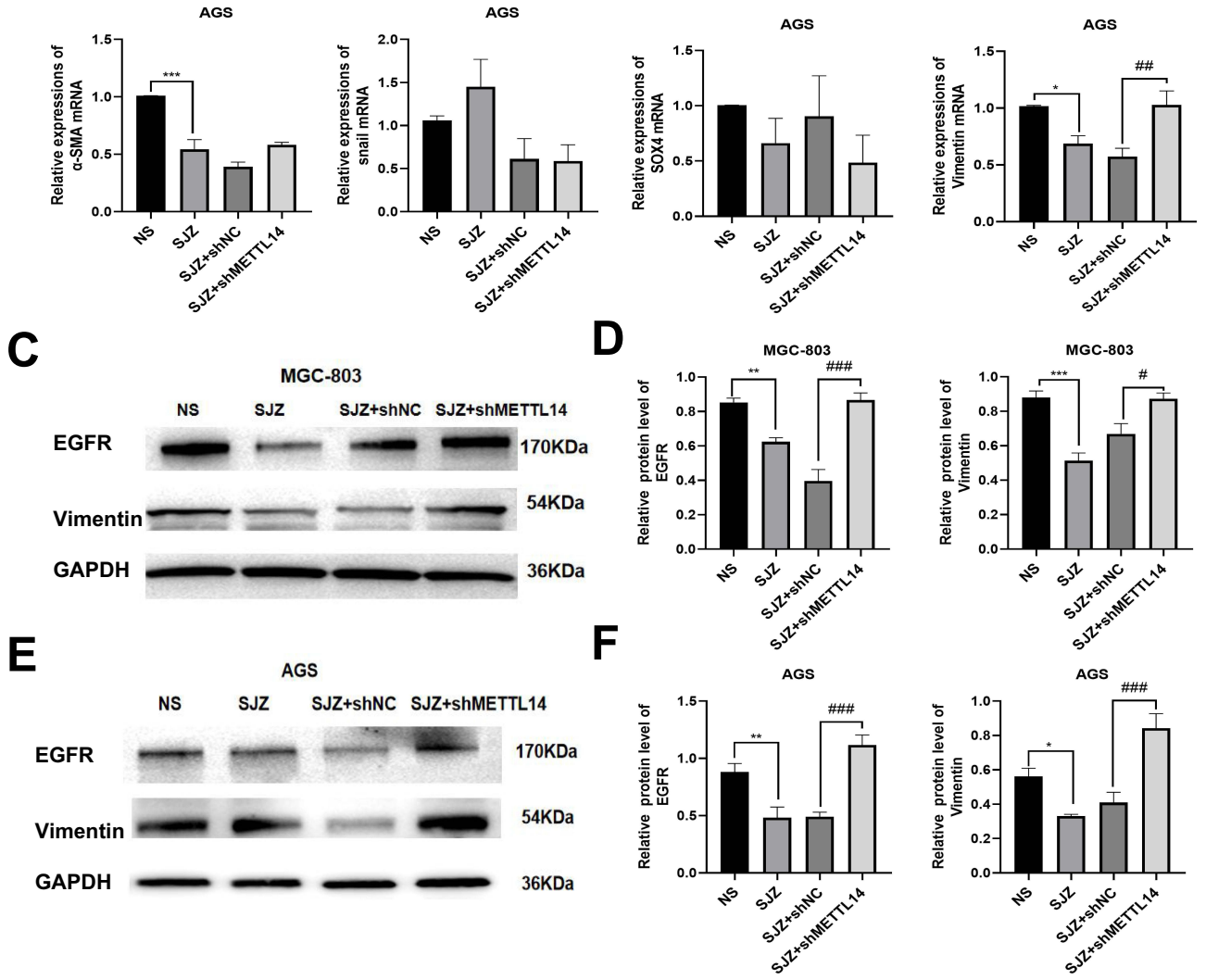

Figure 14 The mRNA expression levels of E-cadherin, S100A4, MMP-9, EGFR, α-SMA, Snail, SOX4, and Vimentin were detected by RT-qPCR in MGC-803 cells (**A**) and AGS cells (**B**) incubation with SJZ after transfection of sh-METTL14 or sh-NC at 48-h. The protein expressions of EGFR and Vimentin in MGC-803 cells (**C** and **D**) and AGS cells (**E** and **F**) were determined by Western blotting. The data are stated as the means±SEM, n=5. **P*<0.05, ***P*<0.01, ****P*<0.001, #*P*<0.05, ##*P*<0.01, ###*P*<0.001 compared to control.

miRNAs in the context of gastric cancer. Subsequent investigations in this domain might offer precious understandings regarding the m6A regulatory routes of miRNAs in SJZ.

PPI analysis of the intersecting targets identified core targets in SJZ treatment of gastric cancer, such as EGFR, TP53, and STAT3. EGFR is a downstream target of METTL3 in hepatocellular carcinoma[48] and ALKBH5 regulates STAT3 activity in an m6A-dependent manner in human osteosarcoma.[49] The present study confirmed that SJZ treatment reduced the expression of EGFR by METTL14. Therefore, we hypothesized that m6A is a crucial mechanism of SJZ in treatment of gastric cancer.

SJZ, a traditional formula used for Qi and Pi invigoration, is closely associated with immune regulation.[30] Our KEGG enrichment analysis suggested that the T-cell receptor signaling pathway may be particularly relevant in the context of SJZ treatment. T-cells play a vital role in the pathogenesis of gastric cancer and function as predictive biomarkers for the prognosis of gastric cancer patients.[50,51] Based on the current state of our understanding, a limited number of investigations have centered on the impacts of SJZ upon T cell receptors. Therefore, our findings are helpful in clarifying the mechanism of SJZ associated with immunity, and the effect of SJZ on T cell receptors should be further explored in the future. In addition, our study has some limitations. It is not clear which herb or active ingredient of SJZ plays a major role in gastric cancer. We found that SJZ may regulate downstream targets through the m6A methyltransferase

https://doi.org/10.2147/DDDT.S506702

METTL14, raising questions regarding the potential of SJZ to inhibit gastric cancer through m6A-dependent mechanisms. Further investigation is needed to elucidate the specific regulatory pathways through which SJZ suppresses gastric cancer and the mechanisms by which it regulates the expression of METTL3/14, both in vivo and in vitro.

Conclusion

We conducted an untargeted metabolomic study and network pharmacology to determine the material basis of SJZ and explore the potential m6A-regulated targets of SJZ for gastric cancer therapy. SJZ prevented clone formation, migration, and invasion of gastric cancer cells by METTL14. These findings have deepened our understanding of the antitumor effect of SJZ and suggest that SJZ has multi-component, multi-target, and multi-pathway characteristics in the treatment of gastric cancer, and that the m6A methyltransferase METTL14 may be a crucial target of SJZ.

Data Sharing Statement

The data used to support the findings of this study have been included in this article. The datasets used and/or analyzed during the current study are available from the corresponding author upon reasonable request.

Acknowledgments

Xiangnan Li and Linlin Zhao are co-first authors for this study. This work was supported by LiaoNing Revitalization Talents Program under Grant No. XLYC2203180; and Science and Technology Plan Joint Program of Liaoning Province (Applied Basic Research Project) under Grant No.2023JH2/101700205; and Traditional Chinese Medicine Multidisciplinary Innovation Team Program of Liaoning Province (LNZYYCXTD-JCCX-002); and Young Scientists Fund of National Natural Science Foundation of China under Grant No. 82405505; and Science and Technology Plan Joint Program of Liaoning Province (PhD Start-up project) under Grant No. 2023-BSBA-218.

Author Contributions

All authors made a significant contribution to the work reported, whether that is in the conception, study design, execution, acquisition of data, analysis and interpretation, or in all these areas; took part in drafting, revising or critically reviewing the article; gave final approval of the version to be published; have agreed on the journal to which the article has been submitted; and agree to be accountable for all aspects of the work.

Disclosure

The authors report no conflicts of interest in this work.

References

1. Smyth EC, Nilsson M, Grabsch HI, et al. Gastric cancer. *Lancet*. 2020;396(10251):635–648. doi:10.1016/S0140-6736(20)31288-5
2. Ajani JA, D'Amico TA, Bentrem DJ, et al. Gastric cancer, version 2. 2022, NCCN clinical practice guidelines in oncology. *J Natl Compr Canc Netw*. 2022;20(2):167–192.
3. Li K, Zhang A, Li X, et al. Advances in clinical immunotherapy for gastric cancer. *BBA - Rev Cancer*. 2021;1876(2):188615. doi:10.1016/j.bbcan.2021.188615
4. Zhao W, Liu Z, Zhang Z, et al. Si Jun Zi decoction inhibits the growth of lung cancer by reducing the expression of PD-L1 through TLR4/MyD88/NF-κB pathway. *J Ethnopharmacol*. 2024;318:116948. doi:10.1016/j.jep.2023.116948
5. Shang L, Wang Y, Li J, et al. Mechanism of Sijunzi decoction in the treatment of colorectal cancer based on network pharmacology and experimental validation. *J Ethnopharmacol*. 2023;302:115876. doi:10.1016/j.jep.2022.115876
6. Han X, Wei Q, Lv Y, et al. Ginseng-derived nanoparticles potentiate immune checkpoint antibody efficacy by reprogramming the cold tumor microenvironment. *Mol Ther*. 2022;30(1):327–340. doi:10.1016/j.ymthe.2021.08.028
7. Shen M, Liu J, Wang K, Hussein AF. Effect of traditional Chinese medicine on allergic rhinitis in children under data mining. *Comput Math Methods Med*. 2022;2022:7007370. doi:10.1155/2022/7007370
8. Yang B, Zhang Z, Song J, et al. Interpreting the efficacy enhancement mechanism of Chinese medicine processing from a biopharmaceutic perspective. *Chin Med*. 2024;19(1):14–23. doi:10.1186/s13020-024-00887-0
9. Tibenda J, Du Y, Huang S, et al. Pharmacological mechanisms and adjuvant properties of licorice Glycyrrhiza in treating gastric cancer. *Molecules*. 2023;28(19).
10. Tang Y, Han T. Effects of Huangqi Sijunzi decoction immune function of patients with advanced primary hepatocellular carcinoma with deficiency of Qi and blood. *J Pract Tradit Chin Intern Med*. 2021;35(09):20–22.

11. Sun X, Ma J, Li Q, et al. Meta-analysis of Sijunzi Tang combined with chemotherapy in improving immune function of patients with malignant tumor. *Asia-Pacific Tradit Med*. 2021;17(06):134–141.
12. Tang B, Wu Y, Cao X, et al. Efficacy of Sijunzi decoction and lts effect on immune function of patients after radical gastrectomy for gastric cancer. *China Pharmaceuticals*. 2022;31(15):104–107.
13. Zhang F, Xie A, Zhang J, et al. Clinical study on the influence of Sijunzi decoction on gut microbiota and immune function of postoperative patients with colorectal cancer chemotherapy. *J Shantou Univ Med Coll*. 2020;33(04):206–208.
14. Li X, Yang Y, Guo S, et al. Effects of serum containing Sijunzi decoction on stemness properties of gastric cancer cells and its mechanism. *J Basic Chin Med*. 2022;28(07):1120–1125.
15. Guo J, Wang D, Cong P, et al. Effects of benefiting qi and strengthening spleen method on proliferation and apoptosis of human gastric cancer MGC803 cells. *Chin J Immunol*. 2019;35(14):1703–1707.
16. Li X, Miao L, Sun H, et al. Mechanism of Sijunzi Decoction on enhancing the anti-gastric cancer effect of cisplatin based on transcriptomics. *China J Tradition Chin Med Pharm*. 2023;38(06):2856–2861.
17. Guo J, Li X, Miao L, et al. High-throughput sequencing reveals the differential MicroRNA expression profiles of human gastric cancer SGC7901 cell xenograft nude mouse models treated with traditional Chinese medicine Si Jun Zi Tang decoction. *Evid Based Compl Alternat Med*. 2021;2021:1–12.
18. Li X, Chen W, Miao L, et al. Antitumor effect of Si-Jun-Zi decoction on SGC7901 gastric cancer cells by CMTM2 activation. *Evid Based Compl Alternat Med*. 2022;2022:4675815. doi:10.1155/2022/4675815
19. Fan H, Chen Z, Chen X, et al. METTL14-mediated m6A modification of circORC5 suppresses gastric cancer progression by regulating miR-30c-2-3p/AKT1S1 axis. *Mol Cancer*. 2022;21(1):51. doi:10.1186/s12943-022-01521-z
20. Gu Y, Wu X, Zhang J, et al. The evolving landscape of N6-methyladenosine modification in the tumor microenvironment. *Mol Ther*. 2021;29 (5):1703–1715. doi:10.1016/j.ymthe.2021.04.009
21. Ding S, Zhang X, Pei J, et al. Role of N6-methyladenosine RNA modification in gastric cancer. *Cell Death Discov*. 2023;9(1):241. doi:10.1038/s41420-023-01485-z
22. Wang Q, Chen C, Ding Q, et al. METTL3-mediated m(6)A modification of HDGF mRNA promotes gastric cancer progression and has prognostic significance. *Gut*. 2020;69(7):1193–1205. doi:10.1136/gutjnl-2019-319639
23. Wang N, Huo X, Zhang B, et al. METTL3-mediated ADAMTS9 suppression facilitates angiogenesis and carcinogenesis in gastric cancer. *Front Oncol*. 2022;12:861807. doi:10.3389/fonc.2022.861807
24. Chen X, Yang Y, Yu Y, et al. CircUGGT2 downregulation by METTL14-dependent m(6)A modification suppresses gastric cancer progression and cisplatin resistance through interaction with miR-186-3p/MAP3K9 axis. *Pharmacol Res*. 2024;204:107206. doi:10.1016/j.phrs.2024.107206
25. Li X, Ma S, Deng Y, et al. Targeting the RNA m6A modification for cancer immunotherapy. *Mol Cancer*. 2022;21(1).
26. Bai Q, Shi M, Sun X, et al. Comprehensive analysis of the m6A-related molecular patterns and diagnostic biomarkers in osteoporosis. *Front Endocrinol*. 2022;13:957742. doi:10.3389/fendo.2022.957742
27. Zhang B, Wu Q, Li B, et al. m(6)A regulator-mediated methylation modification patterns and tumor microenvironment infiltration characterization in gastric cancer. *Mol Cancer*. 2020;19(1):53. doi:10.1186/s12943-020-01170-0
28. Li Y, Liao L, Liu P, et al. Sijunzi Decoction Inhibits Stemness by Suppressing β-catenin transcriptional activity in Gastric Cancer Cells. *Chin J Inter Med*. 2022;28(8):702–710. doi:10.1007/s11655-021-3314-9
29. Zhu Y, Ma R, Cheng W, et al. Sijunzi decoction ameliorates gastric precancerous lesions via regulating oxidative phosphorylation based on proteomics and metabolomics. *J Ethnopharmacol*. 2024;318:116925. doi:10.1016/j.jep.2023.116925
30. Wang X, Pan S, Chen L, et al. Sijunzi decoction enhances sensitivity of colon cancer cells to NK cell destruction by modulating P53 expression. *J Ethnopharmacol*. 2024;329:118115. doi:10.1016/j.jep.2024.118115
31. Li H, Pu X, Lin Y, et al. Sijunzi decoction alleviates inflammation and intestinal epithelial barrier damage and modulates the gut microbiota in ulcerative colitis mice. *Front Pharmacol*. 2024;15:1360972. doi:10.3389/fphar.2024.1360972
32. Zhang D, Duan S, He Z, et al. Sijunzi decoction targets IL1B and TNF to reduce neutrophil extracellular traps (NETs) in ulcerative colitis: evidence from silicon prediction and experiment validation. *Drug Des Devel Ther*. 2023;17:3103–3128. doi:10.2147/DDDT.S428814
33. Wu Y, Zheng Y, Wang X, et al. Ginseng-containing sijunzi decoction ameliorates ulcerative colitis by orchestrating gut homeostasis in microbial modulation and intestinal barrier integrity. *Am J Chin Med*. 2023;51(3):677–699. doi:10.1142/S0192415X23500325
34. Du J, Tao Q, Liu Y, et al. Assessment of the targeted effect of Sijunzi decoction on the colorectal cancer microenvironment via the ESTIMATE algorithm. *PLoS One*. 2022;17(3):e0264720. doi:10.1371/journal.pone.0264720
35. Cai K, Zheng Q, Zhu X, et al. Mechanism of Sijunzi decoction in treatment of Alzheimer's disease based on UPLC-Q-TOF-MS, network pharmacology, and experimental verification. *China J Chin Materia Medica*. 2023;48(06):1620–1631. doi:10.19540/j.cnki.cjcmm.20221209.401
36. Wang Z, Li T, Li R, et al. Sijunzi Tang improves gefitinib resistance by regulating glutamine metabolism. *Biomed Pharmacother*. 2023;167:115438. doi:10.1016/j.biopha.2023.115438
37. Wang D, Wang J, Yan C, et al. Gastrodia elata Blume extract improves high-fat diet-induced type 2 diabetes by regulating gut microbiota and bile acid profile. *Front Microbiol*. 2022;13:1091712. doi:10.3389/fmicb.2022.1091712
38. Liu J, Li Z, Lao Y, et al. Network pharmacology, molecular docking, and experimental verification reveal the mechanism of San-Huang decoction in treating acute kidney injury. *Front Pharmacol*. 2023;14:1060464. doi:10.3389/fphar.2023.1060464
39. Li J, Zhang K, Bao J, et al. Potential mechanism of action of Jing Fang Bai Du San in the treatment of COVID-19 using docking and network pharmacology. *Int J Med Sci*. 2022;19(2):213–224. doi:10.7150/ijms.67116
40. Zhang X, Wang M, Qiao Y, et al. Exploring the mechanisms of action of Cordyceps sinensis for the treatment of depression using network pharmacology and molecular docking. *Ann Transl Med*. 2022;10(6):282. doi:10.21037/atm-22-762
41. Feng D, Li P, Xiao W, et al. N-methyladenosine profiling reveals that Xuefu Zhuyu decoction upregulates METTL14 and BDNF in a rat model of traumatic brain injury. *J Ethnopharmacol*. 2023;317:116823. doi:10.1016/j.jep.2023.116823
42. Zhang Y, Wang R, Tan H, et al. Fufang Zhenzhu Tiaozhi (FTZ) capsule ameliorates diabetes-accelerated atherosclerosis via suppressing YTHDF2-mediated m6A modification of SIRT3 mRNA. *J Ethnopharmacol*. 2023;317:116766. doi:10.1016/j.jep.2023.116766
43. Dang Y, Xu J, Yang Y, et al. Ling-gui-zhu-gan decoction alleviates hepatic steatosis through SOCS2 modification by N6-methyladenosine. *Biomed Pharmacother*. 2020;127:109976. doi:10.1016/j.biopha.2020.109976

44. Zhang H, Qi F, Wang J, et al. The m6A methyltransferase METTL3-mediated n6-methyladenosine modification of DEK mRNA to promote gastric cancer cell growth and metastasis. *Int J mol Sci*. 2022;23(12):6451. doi:10.3390/ijms23126451
45. Liu X, Xiao M, Zhang L, et al. The m6A methyltransferase METTL14 inhibits the proliferation, migration, and invasion of gastric cancer by regulating the PI3K/AKT/mTOR signaling pathway. *J Clin Lab Anal*. 2021;35(3):e23655. doi:10.1002/jcla.23655
46. Alarcón CR, Goodarzi H, Lee H, et al. HNRNPA2B1 is a mediator of m6A-dependent nuclear RNA processing events. *Cell*. 2015;162(6):1299–1308. doi:10.1016/j.cell.2015.08.011
47. Feng H, Yuan X, Wu S, et al. Effects of writers, erasers and readers within miRNA-related m6A modification in cancers. *Cell Prolif*. 2023;56(1):e13340. doi:10.1111/cpr.13340
48. Wang L, Yang Q, Zhou Q, et al. METTL3-m(6)A-EGFR-axis drives lenvatinib resistance in hepatocellular carcinoma. *Cancer Lett*. 2023;559:216122. doi:10.1016/j.canlet.2023.216122
49. Yang Z, Cai Z, Yang C, et al. ALKBH5 regulates STAT3 activity to affect the proliferation and tumorigenicity of osteosarcoma via an m6A-YTHDF2-dependent manner. *EBioMedicine*. 2022;80:104019. doi:10.1016/j.ebiom.2022.104019
50. Wang B, Zhang Z, Liu W, et al. Targeting regulatory T cells in gastric cancer: pathogenesis, immunotherapy, and prognosis. *Biomed Pharmacother*. 2023;158:114180. doi:10.1016/j.biopha.2022.114180
51. Shen D, Pang J, Bi Y, et al. LSD1 deletion decreases exosomal PD-L1 and restores T-cell response in gastric cancer. *Mol Cancer*. 2022;21(1):75. doi:10.1186/s12943-022-01557-1